AEROSOL OPTICAL DEPTH AND ITS RELATIONSHIP TO RADAR DERIVED
PRECIPITATION IN MALI, WEST AFRICA

by

David Benham Keith
Bachelor of Science, Embry-Riddle Aeronautical University, 2005
Bachelor of Science, Northern Illinois University, 2008

A Thesis

Submitted to the Graduate Faculty

of the

University of North Dakota

in partial fulfillment of the requirements

for the degree of

Master of Science

Grand Forks, North Dakota
May
2013

This thesis, submitted by David B. Keith in partial fulfillment of the requirements for the Degree of Master of Science from the University of North Dakota, has been read by the Faculty Advisory Committee under whom the work has been done and is hereby approved.

_____
David Delene, Ph.D., Chairperson

_____
Matthew Gilmore, Ph.D., Committee Member

_____
Cedric Grainger, Ph.D., Committee Member

This thesis is being submitted by the appointed advisory committee as having met all of the requirements of the Graduate School at the University of North Dakota and is hereby approved.

_____
Wayne Swisher, Ph.D.
Dean of the Graduate School

_____
Date

PERMISSION

Title   Aerosol Optical Depth and Its Relationship to Radar Derived Precipitation in Mali, West Africa

Department   Atmospheric Sciences

Degree   Master of Science

In presenting this thesis in partial fulfillment of the requirements for a graduate degree from the University of North Dakota, I agree that the library of this University shall make it freely available for inspection. I further agree that permission for extensive copying for scholarly purposes may be granted by the professor who supervised my thesis work or, in his absence, by the chairperson of the department or the dean of the Graduate School. It is understood that any copying or publication or any other use of this thesis or part thereof for financial gain shall not be allowed without my written permission. It is also understood that due recognition shall be given to me and to the University of North Dakota in any scholarly use which may be made of any material in my thesis.

David B. Keith
May 2013

TABLE OF CONTENTS

LIST OF FIGURES

vii

LIST OF TABLES

ACKNOWLEDGMENTS

ABSTRACT

The research goal is to determine if a relationship exists between Aerosol Optical
Depth (AOD) and radar-derived precipitation in Mali, a country located in West Africa.
Precipitation parameters derived from 2006, 2007 and 2008 C-band radar measurements
are compared against Noon to 2 p.m. averaged AOD measurements. The AOD and
Angstrom Exponent (AE) are from an Aerosol Robotic Network (AERONET) site
located 240 km northeast of Bamako, and radar cell (20 dBZ threshold) tracks are
generated using the Thunderstorm Identification, Tracking, Analysis and Nowcasting
radar software (TITAN). Only isolated TITAN cells are used in the analysis. In addition,
environmental filters are applied so that only cases with large Convective Available
Potential Energy (CAPE) and weak 0 to 6 km Above Ground Level (AGL) vertical speed
shear are included in the analyzed dataset to increase the likelihood of isolated convective
cells. Additionally, only cases with low Lifting Condensation Level (LCL) are used to
increase the likelihood of surface-based convection. Days with an Angstrom Exponent
(AE) less than or equal to 0.35 are removed to reduce the influence of desert dust. With
the exclusion of low AE days, an increase in AOD is assumed to imply larger aerosol
concentrations in the lower troposphere.

Analysis of the filtered data set shows a significant negative relationship between
AOD and number of cells per day; a p-value of 0.009 and R^2 of 0.20 indicate a one
percent probability that the slope occurred by chance and that 20 % of the decrease is due

to AOD, respectively. In contrast, linear regressions of each of the following are not statistically significant: AOD versus precipitation flux per cell, AOD versus duration per cell and AOD versus precipitation flux per day. Based on linear regression analysis between non-dust AOD (aerosol burden) and radar data, the conclusion is made that increased concentrations of aerosols result in fewer storm cells (perhaps because it is more difficult for initial clouds to produce precipitation-sized drops); however, the aerosol burden does not affect the amount of precipitation produced by individual detected cells that are able to form. These results, as well as previous studies, suggest that Mali's operational weather modification program should concentrate its resources by conducting hygroscopic seeding on days with high AE and AOD because it is those days that clouds would benefit the most from a broadening of the cloud drop size distribution.

CHAPTER I

INTRODUCTION

Mali lies within a region of West Africa (Fig. 1) where rainfall variability has been documented to be an ongoing influence on farmers and the general population for the last two thousand years (Nicholson 2001). Mali could experience economic losses due to increased rainfall variability from $70 to $142 million over the period 1996 to 2030 (Butt et al. 2005). Kurulasuriya et al. (2006) conducted an economic analysis of 9,000 farmers in 11 African countries and predicted that farm revenues would fall due to increased rainfall variability. Additionally, by the year 2030 hunger could increase from its current level of 34 %, as a proportion of Mali's population, to between 64 and 72 % due to increased rainfall variability (Butt et al. 2005).
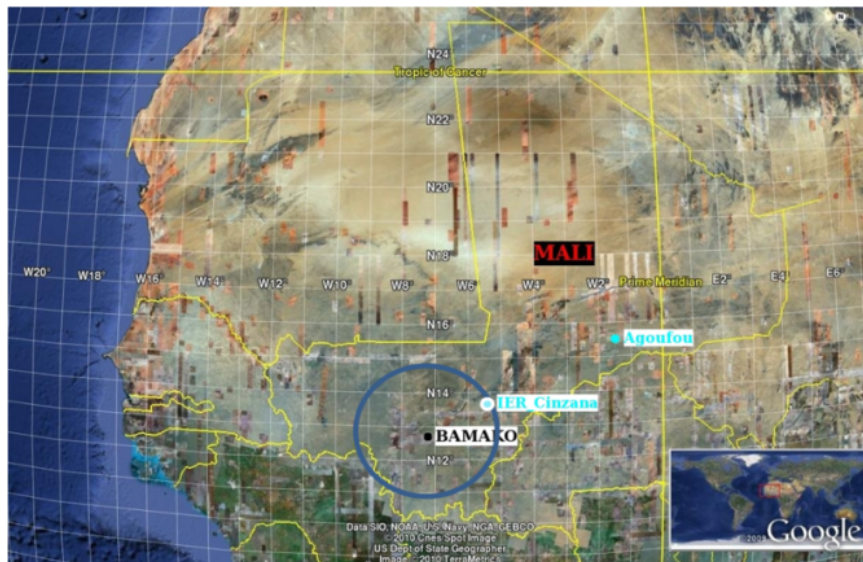
Figure 1. Google Earth image of the Mali region that shows the approximate radar coverage area (large blue circle) and the active Aerosol Robotic Network (AERONET) sites (small blue filled circles).

1

The threats of economic loss and hunger in Mali have spurred the development of various economic, biophysical and policy adoptions to mitigate the impact of rainfall variability (Butt et al. 2005). People in Mali move their cattle from a region receiving less rainfall to one receiving more rainfall and use drought resistant crops to overcome the high degree of rainfall variability. Rainfall augmentation, referred to as "cloud seeding" henceforth, is another method that Mali is using to limit the negative impacts of rainfall variability on people's livelihoods and survival.

Cloud seeding typically involves using ground or aircraft based release systems that burn a flammable dry material or liquid based solution, which produce particles that water vapor can condense upon or liquid water can freeze upon. Two widely used aircraft based cloud seeding technologies are called hygroscopic and glaciogenic. Glaciogenic seeding involves deployment of ice nuclei in regions of super-cooled water to produce ice. Hygroscopic seeding releases course mode (2 to 5 µm in diameter) salt, or other hygroscopic material, into updrafts at the base of warm or mixed phase clouds (Cotton 2007). Flares attached behind the aircraft wing are burned to produce the hygroscopic particles, which are good cloud condensation nuclei (CCN). Water vapor condenses onto larger CCN in the cloud updraft to form droplets earlier than onto smaller CCN. The larger size aerosols produced by hygroscopic flares activate before smaller sized aerosols occurring naturally, which broaden the cloud droplet size distribution produced during condensational growth. This is in contrast to having smaller sized CCN activate which produce a larger number of droplets, a smaller cloud droplet mean volume diameter and a narrower droplet size distribution. A narrower drop size distribution adversely affects the ability of warm or mixed phase clouds to produce precipitation by

2

decreasing the efficiency of the collision-coalescence process. Modeling results have shown that hygroscopic seeding produces rain earlier within a typical cumulus lifetime of 30 minutes (Levin and Cotton 2009). Mather (1991) detected the hygroscopic seeding effect through radar observations of developing clouds downwind of a South Africa paper mill where emissions of course mode particles acted as Giant (> 1 μm) Cloud Condensation Nuclei (GCCN).

The effectiveness of cloud seeding operations is not agreed upon within the scientific community and there are many opinions on the potential or success of cloud seeding. The American Society of Civil Engineers (ASCE) published a report entitled, "Standard Practice for the design and Operation of Precipitation Enhancement Projects" (ASCE 2004). ASCE (2004) developed its position concerning cloud seeding from a review of statements and research conducted and published independently by the American Meteorological Society (AMS), Weather Modification Association (WMA), and World Meteorological Organization (WMO). The ASCE supports and encourages the continued study of weather modification and claims that increasing demands on water resources due to population growth have reduced the ability of nations to provide adequate water resources (ASCE 2004). Cloud seeding could be one of the tools used to augment naturally occurring water resources (ASCE 2004).

Silverman (2003) provides an excellent review of four hygroscopic cloud seeding projects. Results of experiments in South Africa, Mexico, India and Thailand showed statistically significant increases in rain-gauge measurements of precipitation in seeding areas compared to control areas. Results from numerical cloud model calculations showed that hygroscopic seeding could act to accelerate condensation and the subsequent

3

collision-coalescence process, which promotes earlier development of precipitation-size drops (Silverman 2003). However, Silverman (2003) declared that evidence to support the precipitation increase observed in South Africa, Mexico and Thailand experiments was not justified by the projects' original hypotheses. The projects' hypotheses were based on microphysical effects alone, and in order to justify the increases in precipitation, seeding-induced dynamic effects had to be considered as well. Two examples of dynamic effects are: 1) Stronger updrafts encouraged by increased latent heat due to increasing collisions and coalescences, and 2) Seeding producing rainfall earlier in clouds, which would cause a stronger and more localized downdraft to develop a stronger gust front that would initiate more new vigorous cloud development. Physical observations are lacking in the four experiments discussed by Silverman (2003); therefore, the seeding-induced dynamic effects are speculative. Silverman's (2003) point is that the results are not explained by a project's conceptual model, and a conclusion should not be made that seeding was responsible for the observed rainfall increase. Silverman (2003) recommended that evaluation criteria be based on physical cloud observations rather than a statistical comparison between rain gauges within a control and seeding area. Physical observations are important because they link the physical chain of events associated with the seeding conceptual model.

Since conducting cloud seeding is expensive; therefore, leaders of Mali's program would benefit from better knowledge of the most efficient environment to conduct cloud seeding so personnel, flight time and seeding material are used when they have the greatest chance of being effective. Mali conducted a feasibility study from 2006 through 2008. Radar measurements collected during 2006 and 2007 indicated large interannual

variability in storm characteristics. According to Kucera et al. (2008), there are ample opportunities for cloud seeding targets in Mali. Results from aircraft-based cloud measurements show that the cloud characteristics satisfy one of the criteria for hygroscopic seeding: narrow cloud base droplet spectrum and high concentration of droplets. However, the droplet size distributions are typically broad enough in the days immediately following heavy rain events, rendering hygroscopic seeding unnecessary (Kucera et al 2008). Therefore, a measure of the atmospheric aerosol burden, termed Aerosol Optical Depth (AOD), is investigated as a decision making tool that could help determine those days most appropriate for conducting hygroscopic cloud seeding in Mali. In order to determine if AOD is a useful tool, the relationship between AOD and rainfall derived by radar on a cell-by-cell basis is analyzed.

To determine how cloud seeding could help Mali's augmenting precipitation, it is important to first understand the country's climatological rainfall patterns. Figure 2 shows that Mali has four main climate regions where annual rainfall ranges from 1500 mm in the southwest to 50 mm in the North (Nicholson 2001). Table 1 indicates that the monthly rainfall peak shifts northward during the rainy season (June, July, August and September). In August for example, the monthly rainfall percentage increases from 3 % in the lower latitude region (4 to 6 °N), to 12 % in the middle latitude region (12 to 14 °N), to 41 % in the higher latitude region (18 to 20 °N).

Figure 2. Google Earth image of Mali's climate regions (left image) and average annual rainfall (mm/year) amounts (right image). The rainfall contours are based on 20th century rain gauge data that are adapted from Nicholson (2001).

Table 1. Mean annual rainfall (right-most column in mm yr^{-1}) for 2 ° latitudinal sectors in West Africa based on rain gauge measurements from 1901 to 1998. The percentages represent the ratio of monthly mean to annual mean rainfall averaged for stations in each latitudinal sector listed. August (bold faced font) contributed most to the mean annual rainfall for latitudes greater than 10 °N. Latitude sectors between 10 °N and 16 °N are in bold font to indicate that they represent the approximate latitudinal area covered by the Bamako radar. Table adapted from Nicholson et al. (2000).

Latitude	May	Jun	Jul	**Aug**	Sep	Oct	Nov	Mean
18-20 °N	2 %	6 %	15 %	41 %	23 %	5 %	2 %	84 mm yr^{-1}
16-18 °N	1 %	7 %	23 %	40 %	22 %	5 %	0 %	255 mm yr^{-1}
14-16 °N	2 %	8 %	24 %	**38 %**	22 %	5 %	0 %	498 mm yr^{-1}
12-14 °N	5 %	12 %	23 %	**32 %**	20 %	6 %	1 %	843 mm yr^{-1}
10-12 °N	8 %	12 %	19 %	**25 %**	20 %	9 %	2 %	1368 mm yr^{-1}
8-10 °N	9 %	12 %	17 %	18 %	18 %	10 %	3 %	1466 mm yr^{-1}
6- 8 °N	11 %	16 %	12 %	10 %	14 %	12 %	5 %	1564 mm yr^{-1}
4- 6 °N	16 %	24 %	9 %	3 %	6 %	9 %	8 %	1810 mm yr^{-1}

Interannual rainfall was studied in Nicholson et al. (2000) using a standardized annual departure from the overall mean. Nicholson et al. (2000) calculated that the western region of West Africa, which includes Mali, received 200 to 500 mm more rainfall annually between the 1931 and 1961 period compared to the 1970 and 1997 period. The overall average rainfall for West Africa from 1968 to 1997 was 100 to 200 mm less than 1930 to 1960. August rainfall in the Sahel, Soudan and Soudano-Guinean climate regions was 55 %, 37 %, and 26 % below average, respectively, for the period

1968 to 1997 compared to 1930 to 1960 (Nicholson 2000). The transition from the 1931 to 1960 wet period to the 1970 to 1997 dry period was not sudden as there was a steady decrease in annual rainfall from the 1950s to the early 1980s. Starting in the early 1980s, annual rainfall began to increase until it leveled records leveled at above average in the early 2000s (Nicholson 2005). Overall, Mali has experienced rainfall variability throughout the 20th century.

In the context of rainfall augmentation through cloud seeding, one should understand the synoptic and dynamic mechanisms responsible for the location of the rain band present over Mali from July through September (Nicholson 2009). Henceforth, the term 'rain band' denotes the position of the rainfall whereas intertropical convergence zone (ITCZ) (Zhang et al. 2006; Nicholson 2009) denotes the convergence zone of surface winds. Remote sensing studies' (Ba et al. 1995; Adler et al. 2000; Sultan and Janicot 2003) using rain belt clouds to delineate the position of the ITCZ is ambiguous according to Nicholson (2009). In line with Nicholson (2009), the term ITCZ is used to reference the point of convergence between the Northerly and Southerly meridional flows that shift from 10 °N in January to 20 °N in August (Nicholson and Grist 2003). The rain band begins its move northward from the Guinean coast in February, reaches the Sahel region by late June, and resides over the Sahel region until October. In October, the rain band begins moving southward reaching the Guinean coast by December (Sultan and Janicot 2000; Le Barbe et al. 2002; Sultan and Janicot 2003).

Lift, moisture and instability are meteorological ingredients necessary for convective rain cells; whereas, vertical-shear is not an ingredient necessary for storm initiation, but is correlated to storm type (Weisman and Klemp 1982). These ingredients

7

are controlled by three quasi-independent mechanisms that influence precipitation development over West Africa: ascent linked to the upper level jet streams, convergence associated with the surface ITCZ and a coastal circulation cell linked to sea-breeze (Nicholson 2009). Figure 3 illustrates the classical and updated views on weather patterns that affect West Africa precipitation. The primary rain producing mechanism pertinent to Mali is the strong core of ascent lying between the axes of the African Easterly Jet (AEJ) and the Tropical Easterly Jet (TEJ). For ascent to produce clouds through expansion and cooling of individual volumes of air, known as air parcels, there must be adequate moisture in the low-level environment. Figure 3 shows that one low-level moisture source is the southwesterly monsoonal flow; however, Nicholson (2009) stated that moisture is more often obtained from soil evaporation.

Figure 3. The left image is a classic depiction of a weather pattern associated with the monsoon flow over the West Africa region. The right image is a modified depiction of the left image showing the weather pattern associated with the monsoonal flow over the West African region. The acronyms listed in the figure are as follows: Divergence (DIV), Convergence (CONV), Inter-tropical Convergence Zone (ITCZ), African Easterly Jet (AEJ), and Tropical Easterly Jet (TEJ). The points A, B, C and D are from Nicholson (2009) and not important to the research presented in this thesis. Images are adapted from Nicholson (2009).

Aerosols are important for precipitation formation, which motivates the main goal of this study: to understand the relationship between AOD, in the absence of hygroscopic cloud seeding, and radar derived precipitation. Solid and liquid particles that are suspended in the atmosphere are defined as Aerosols. They range from 0.001 um to 20.0 um in diameter (Levin and Cotton 2009; Rogers and Yau 1989) and are classified into three size modes: nucleation (diameter < 0.1 um), accumulation (0.1 um < diameter < 1.0 um) and course (diameter > 1.0 um) (Pruppacher and Klett 1997). Aerosols' size distributions and chemistry are typically related to the source region. Smoke from forest fires and pollution from anthropogenic emission are two sources of atmospheric aerosols (Dennis 1980). Two important aerosol source regions for Mali are the Sahara region to the north that produces course mode aerosols by wind blowing across the dry desert land and the Central Africa region to the south that produces accumulation mode aerosols from forest fires. AOD is a proxy for atmospheric aerosol concentration since it is the vertical integration of aerosol extinction. AOD provides a direct inference of number concentration when the aerosol chemical composition and size distribution are constant (Nowofor 2010).

The aerosol-cloud-climate system is comprised of a multitude of feedbacks that make predicting radiative responses of clouds to changes in aerosol properties difficult (Jiang and Feingold 2006). There are aerosol indirect effects that influence the formation of clouds and the development of precipitation. The first aerosol indirect effect describes the response of cloud drop size and cloud reflectance to a change in aerosol concentration while holding liquid water content (LWC) constant (Twomey 1974). The second aerosol indirect effect describes how an increase in aerosol concentration reduces the ability of a

cloud to precipitate, increases cloud LWC, increases coverage and extends cloud lifetime (Albrecht 1989). The aerosol semi-direct effect describes how the presence of aerosol results in decreased insolation, which in turn influences cloud and precipitation production. The Jiang and Feingold (2006) modeling results indicated that increases in accumulation mode aerosols resulted in smaller effective cloud droplet radii and reduced surface precipitation – the second indirect effect. Precipitation was reduced by decreases in droplet radii, which resulted in fewer collisions and subsequent coalescences. Simulations where one aerosol effect is isolated from other effects should be interpreted with caution because there are aerosol semi-direct and indirect effects occurring at the same time. Jiang and Feingold (2006) additionally performed a simulation that only included aerosol semi-direct effects where by increased aerosol concentration resulted in a 26.5 % reduction in incoming solar radiation. The reduction in incoming solar radiation produced a decrease in surface heat flux and consequently weaker convection, much shallower clouds, and lower cloud cover compared to the simulation that did not include the aerosol semi-direct effect. Therefore, due to the complexity of the influence that aerosols have on cloud and precipitation production, it is important to evaluate modeled aerosol effects using atmospheric measurements. Hence, the research objective is to understand the influence that AOD, taken to represent aerosol number concentration, has on radar derived precipitation, taken to represent surface precipitation.

CHAPTER II

DATA AND INSTRUMENTATION

Three instruments provided the main datasets for this study: 1) AOD and AE data from an Aerosol Robotic Network (AERONET) site, 2) precipitation data from Weather Surveillance Radar (WSR100) measurements, and 3) CAPE, LCL, and 0-6 km vertical speed shear calculated from the Bamako, Mali 12 UTC (noon local time) radiosonde measurements. AERONET is comprised of approximately 200 model CE-318A sun/sky radiometers that are manufactured in Paris, France by the company CIMEL. Mali's rainfall enhancement project used a WSR-100 C-band radar manufactured by the Enterprise Electronics Corporation that was located at 12.54 °N, 7.95 °W and 390 m Mean Sea Level (MSL) elevation. Radiosondes were launched twice daily from Bamako Mali.

The radiometers within AERONET measure direct and diffuse sky radiance during daylight hours to obtain total column integrated aerosol optical properties, i.e. AOD. Direct sun measurements are made every 15 minutes in eight spectral bands between 340 and 1020 nm (Holben et al. 2001). The IER Cinzana AERONET site used for this research is located 240 km east-northeast (on average upwind) of the Bamako radar (Fig. 4). Level 2.0 IER Cinzana AERONET data were downloaded (saved with the "060101_081231_IER_Cinzana.lev20_noheader" filename) from the NASA AERONET web portal (Holben 2012). Level 2.0 data has the highest level of quality assurance

11

performed on it. The quality assurance includes removing data due to cloud contamination, which is discussed in GSFC 2012; however, the specifics are beyond the scope of this research.

Figure 4. The AERONET instrument at the IER Cinzana site in rural Mali, West Africa is located on a concrete platform in a cultivated region.

The WSR100 wavelength is 5.35 cm with a beam width of 1.6 °. The radar scan-strategy incorporated beam elevation angles of 0.5, 1.5, 2.5, 3.5, 4.5, 6, 8, 11, 15, 22 and 32 degrees resulting in a volume scan time of 240 s. Thunderstorm Identification, Tracking, Analysis, and Nowcasting (TITAN) radar software (Dixon 2010) was used to transform raw radar data into polar coordinates, apply noise filters and convert to a Cartesian grid spacing (Dixon and Weiner 1993). The following paragraph describes the processing completed in Mali that was setup using TITAN parameterization files.

Polar coordinate beam data ingested by TITAN are flagged valid only if the angle is within 0.45 ° of the target elevation angle, which prevents recording data when the antenna drops down for a new volume scan. There is no maximum range limit flag set for the radar data. Volume scans exceeding 900 seconds are not saved to prevent cases where the data stream or volume scan is interrupted. Initiation of a new cell-track history is done when the time between volume scans is greater than 1200 s. The polar data is passed through a Normalized Coherent Power (NCP) filter where the mean power at each pulse is divided by the total transmitted power. The radar data is deemed valid if the NCP is greater than 0.5 and the power greater than -95 dB. A signal-to-noise (SN) filter is applied to the polar data where SN must be greater than five to be valid. The number of contiguous radar gates along an azimuth with a valid SN is considered a "run." The run length has to exceed five gates to be accepted; otherwise, the respective beam is flagged as missing. Missing beams with respect to the azimuth angle are filled in by interpolation using two adjacent valid beams. After filling in missing azimuth beams, missing elevation beams are replaced by interpolation using two adjacent valid elevation angles. The valid polar data is translated to Cartesian grid planes using an 8-point bilinear interpolation where at least four points need to be valid. The Cartesian grid dimensions are 503 km by 503 km by 26 km where the vertical domain begins at 1 km MSL. TITAN performs cell identification and tracking using the Cartesian data.

Data analysis is limited to the rainy season in Mali (1 June to 31 October) and restricted to 2006-2008 because of the availability of high quality radar data. Sounding data were obtained online (http://www.esrl.noaa.gov/raobs/) where 14 June 2008 to 27 October 2008 was the only period missing. An in-operative balloon fill station caused

the gap in sounding data. There was a data gap in AERONET data during August 2006 for unknown reasons. Three days of radar data, 12, 15 and 16 August 2006, were removed during processing because of field operating settings that produced poor quality images or large time gaps when the radar was not transmitting or receiving. Radar data for the day June 7, 2007 was removed because five hours were missing during 13:00 to 21:00 local time. Ultimately, there were 173 days where both valid AERONET and radar data existed on the same day, and 34 days where AERONET, radar and sounding data existed on the same day and passed all of the filtering criteria described in chapter IV.

CHAPTER III

METHODOLOGY

Aerosol Robotic Network

The most comprehensive ground-based instrument to assess the atmospheric aerosol burden is AERONET (Eck et al. 1999). However, AERONET cannot determine layering. Lower tropospheric aerosols typically dominate AOD measurements (Delene and Deshler 2001; Dennis 1980) and aerosol extinction correlates with CCN concentration (Jefferson 2010). Furthermore, Andrea (2009) found that a power law fit to co-located AOD-CCN measurements had an R^2 of 0.88. Therefore, it is reasonable to use AOD to represent below-cloud-base CCN concentration and address the general question: "Do changes in aerosol concentration influence the production of surface based precipitation?" To address this question specifically, the following four relationships are investigated: AOD-Precipitation Flux per a Cell's Lifetime, AOD-Precipitation Flux per Day, AOD-Cell Duration and AOD-Cells per Day.

Mali can have layers of desert dust (course mode aerosols), which would increase the AOD but not influence CCN concentrations below cloud base. Therefore, the AOD-precipitation analysis presented in Chapter IV excludes dust events by using the AERONET Angstrom Exponent (AE) measurements. AE is sensitive to aerosol size and indicates the presence of course mode aerosols (O'Neill et al. 2001). Some researchers (Lesins and Lohmann 2003) use an AE that is greater than one to distinguish between fine and course mode dominated observations. However, Toledano et al. (2008)

determined that the AE is equal to, or less than, 0.35 for desert dust in Morocco (~3000 km north of Mali). A threshold of 0.35 is chosen for the Mali dataset because it is believe that the Mali environment is comparable to Morocco. The AERONET AOD measurements enable calculation of the AE using the following equation:

$$AE_{440/675\,nm} = \frac{log\left(\frac{AOD_{440\,nm}}{AOD_{675\,nm}}\right)}{log\left(\frac{675\,nm}{440\,nm}\right)},$$
(1)

where $AOD_{440\,nm}$ and $AOD_{675\,nm}$ are the AOD at 440 nm and 675 nm wavelengths, respectively. Equation 1 is derived from a relationship presented in Eck et al. (1999). The AOD-CCN relationship found by Andrea (2009) used AOD at 500 nm. Therefore, the research presented in this thesis uses AOD at 500 nm, which is calculated using:

$$AOD_{500\,nm} = AOD_{440\,nm}\left(\frac{440\,nm}{500\,nm}\right)^{AE_{440/675\,nm}}$$
(2)

AOD and AE averages from 12:00 to 14:00 local time are used in the analysis since this is typically the closest period before afternoon cloud development precludes valid measurements. The analysis does not include days with a 12:00 to 14:00 AE average below 0.35 because of the possible influence of desert dust.

Radar

The TITAN software can identify and tracks distinct storm entities referred to as cells. Cells are defined as regions with reflectivity in excess of 20 dBZ (Fig. 5) and less than 80 dBZ. Using a 20 dBZ lower limit instead of TITAN's default 30 dBZ lower limit ensures tracking begins in a cell's infancy and provides a comprehensive data set with respect to duration and rainfall parameters. The method by which TITAN defines a cell and processes radar data begins with identifying adjacent Cartesian grid cells that meet

minimum and maximum dBZ criteria.   Adjacent cells meeting the dBZ criteria are considered "runs" of data in the east-west direction.   "Runs" in this case are in an x-y Cartesian grid space.   Cells are a set of east-west "runs" adjacent in the north-south direction and are required to have a minimum overlap of one grid unit between "runs". To characterize the overlap of cell shapes at successive scan times, two fractions are computed: 1) the overlap area divided by the cell area at time one, and 2) the overlap area divided by the cell area at time two.   The overlap is not valid if the sum of the overlap fraction between the two scans is less than 0.3.   Perfect overlap results in a sum of 2.0, and no overlap results in a sum of 0.0.   For overlap fractions of 0.3 or greater, cells detected at two successive times are grouped into a cell-track.   If the time between two volume-scans is longer than 1200 s (default value for "break time"), such as would occur if the radar was stopped due to maintenance, all track histories end and new ones are started.   There would be lesser overlap with longer break times possibly resulting in an artificially high cell count.   No assessment was conducted on using different maximum allowable break times since evaluation of the TITAN cell-tracking algorithm is beyond the scope of this paper.   However, double counting of cells is not expected to be a problem because reported radar maintenance or interruptions did not occur on any of the 34 days used in the final analysis presented in this paper.
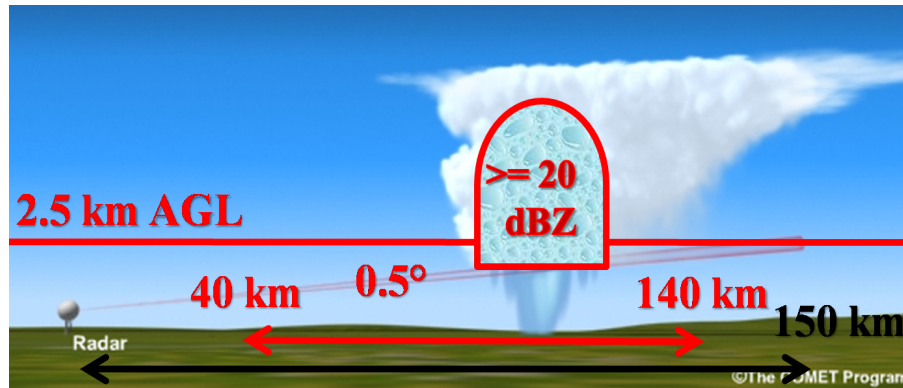
Figure 5. Schematic depicting distance envelop and minimum reflectivity threshold used for valid TITAN cells, base angle of radar and precipitation plane used for calculating precipitation flux falling out of a TITAN cell's base. Image adapted from COMET (2011).

TITAN performs orientation and shape tests to identify second-trip-echo contamination. An elongated low-altitude cell with a major axis aligned along the radial of the radar indicates a possible second trip echo. For a cell to be considered second trip, the radar return has to pass all of the following tests: 1) the horizontal aspect ratio has to exceed four, 2) the vertical aspect ratio has to exceed four, 3) the horizontal orientation has to lie along the orientation of the radar beam, and 4) the beam has to be aligned within 10 ° of the storm's long axis azimuth.

TITAN cell tracks that pass all artifact tests are used in precipitation calculations. Precipitation is calculated at each grid point within a cell's valid area and at height of 2.9 km MSL (2.5 km AGL) (Fig. 5). The 2.9 km MSL height ensures that there is a radar measurement below 2.9 km MSL level out to 140 km. Ensuring a lower level measurement guarantees at least two points (one upper and one lower) are available for interpolating to the Cartesian grid. The 2.9 km MSL level also provides an appreciable range envelope that is not detrimental to the quantity of cells available for the analysis. Precipitation is only calculated if the base of a cell lay at or below 2.9 km MSL. The

precipitation falling out of the base of a TITAN cell is computed using the Sauvageot and Lacaux (1995) equation for radar reflectivity factor (Z):

$$Z = 364R^{1.36},$$ (3)

where R is the precipitation rate. R has units of mm hr^{-1} and Z has units of mm^6 m^{-3}. This relationship is based on data obtained in West Africa's continental regions of Niger and Congo. No study relating radar and rainfall data exists for Mali, which is located in a continental region of West Africa; therefore, eq. 2 is used in place of the Marshal-Palmer Z-R relationship.

Inverting eq. 3 and using Z, the points at height of 2.5 km AGL are used to compute R at each respective grid point contained within the projected cell area. R is integrated over the area of a cell's grid points at 2.5 km AGL to obtain the precipitation flux (m^{3}s^{-1}), which is defined as the depth of liquid that descends through the base area of a respective cell in one second.

TITAN automatically performs a number of final checks to ensure cell tracks are isolated (referred to henceforth as "simple"). Simple cell tracks do not split to form two cells or merge to form one cell. Merged or split cell cases are not used to ensure a greater likelihood of a cell being initiated by surface based convection. Cells are also required to have lifetimes greater than 900 s, a volume between 10 km^3 and 1x10^8 km^3, an initial volume less than 50 km^3 and a maximum speed of 100 km hr^{-1}. Cells that passed all TITAN tests are processed by a custom MATLAB script to subject cell-tracks to the following checks: 1) Exist wholly between the hours of 13:00 and 21:00 local time, 2) lay wholly between 40 and 140 km (Fig. 5) from the Bamako radar, 3) have an average speed greater than 0 km hr^{-1}, 4) have an average precipitation area greater than 0 km^2 and 5)

have a difference between the radar top and base height greater than 0 km. Cell-tracks that do meet these criteria are used to produce the four main analysis parameters: 1) Precipitation flux per cell, 2) Precipitation flux per day, 3) Duration per cell and 4) Cells per day. The precipitation flux per cell ($m^3 s^{-1}$) at each available time step is multiplied by the average volume scan time of 240 seconds to produce the precipitation flux per cell per volume scan $m^3(4 min)^{-1}$. Summing up a cell's precipitation fluxes gives the total precipitation flux per cell (m^3 cell-liftime^{-1}). Adding up all of the precipitation-flux-per-cell for a day produces the precipitation flux per day ($m^3 day^{-1}$). Cells-per-day is obtained simply by tallying all of the cell-tracks on a day. Because each volume scan time is 240 s (or 4 min), then multiplying the number of volume scans in a cell's lifetime by four produces cell-track duration in minutes (min cell^{-1}). TITAN software does not record missing scan information; however, the only reason for a missing scan would be if the radar had a malfunction. The radar maintenance records were reviewed, and no days where a malfunction or interruption is reported are used for the final analysis presented in this paper. Therefore, the probability is low for a cell to be counted as two different cells.

The AOD-Precipitation analysis is restricted to include only TITAN cells that existed wholly between 13:00 and 21:00 local time to increase the chances that cell are from surfaced based convection. In addition, Convective Available Potential Energy (CAPE) ($J kg^{-1}$), Lifting Condensation Level (LCL) (km AGL) and 0.5-6.0 km AGL vertical speed shear (shear) ($m s^{-1}$) are used to restrict the AOD-Precipitation analysis to only surface based convection. Mali balloon soundings provide data to calculate CAPE, LCL and shear. CAPE is calculated using George Bryan's (Bryan 2008) software, which assumes a surface-based reversible parcel. The LCL is defined as the lowest level where

20

the water vapor mixing ratio of the environment immediately surrounding an air parcel is greater than the parcel's saturation-mixing ratio. Shear is the vector difference between average wind in the 0.0 to 1.0 km AGL layer and 5.5 to 6.5 km AGL layer (Weisman and Klemp 1982). The thresholds for CAPE and shear are chosen based on work by Weisman and Klemp (1982) that found the majority of single cell convection occurs when CAPE is greater than 1000 J Kg^{-1} and shear is less than 30 m s^{-1}. The LCL threshold, 2.5 Km AGL, was chosen because it is close to ground level; however, no study was found or sensitivity study conducted to test the validity of the chosen level for insuring surface-based simple-cell convection.

CHAPTER IV

RESULTS AND DISCUSSION

Climatology of Aerosol Optical Depth and Angstrom Exponent

Seasonal changes in the AOD and AE are evident in multi-year long time series AERONET measurements in Mali (Figs. 6 and 7). AOD is highest during late January to late June, which is likely due to aerosol transport within a wind known as the Harmattan. The Harmattan wind is a long-range transport mechanism that brings aerosols (desert-dust amongst them) to Mali during its drier period (Adeyewa and Balogun 2003; Pinker et al. 1994). The majority of rainfall occurs during July through September with the adjacent months, June and October, receiving most of the remaining rainfall (Nicholson 2009). Figure 6 shows that lower AOD persists during July through September. The lower summer time AOD may be due to precipitation processes removing aerosols. Figure 8 shows that there is generally an inverse relationship between AOD and AE; however, the relationship is not without exception because of the uncorrelated influences of the fine and course aerosol modes. Higher AE implies an absence of course mode aerosols and that accumulation mode aerosols are responsible for the increase in AOD. Days dominated by accumulation mode (higher AE) aerosols with higher CCN concentrations (higher AOD) are good candidates for hygroscopic seeding according to the conceptual models discussed previously.
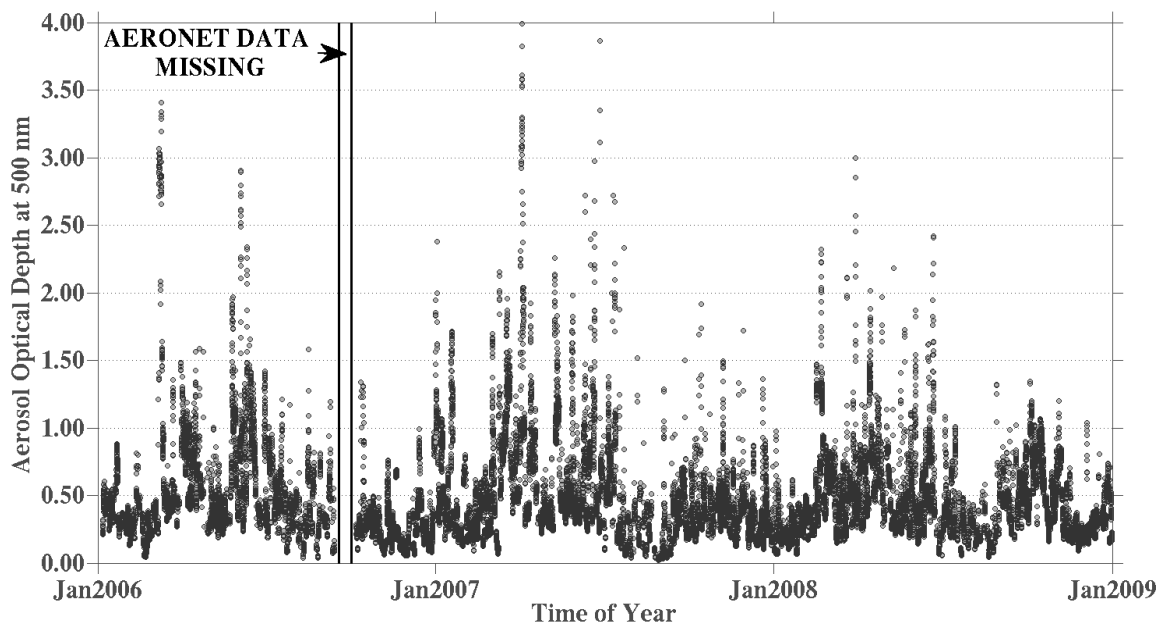
Figure 6. Time series plot of the Aerosol Optical Depth at the IER Cinzana AERONET site. All available 675 nm and 440 nm Level 2.0 data is used to calculate the plotted 500 nm Aerosol Optical Depth. Measurements are conducted every 15 minutes.
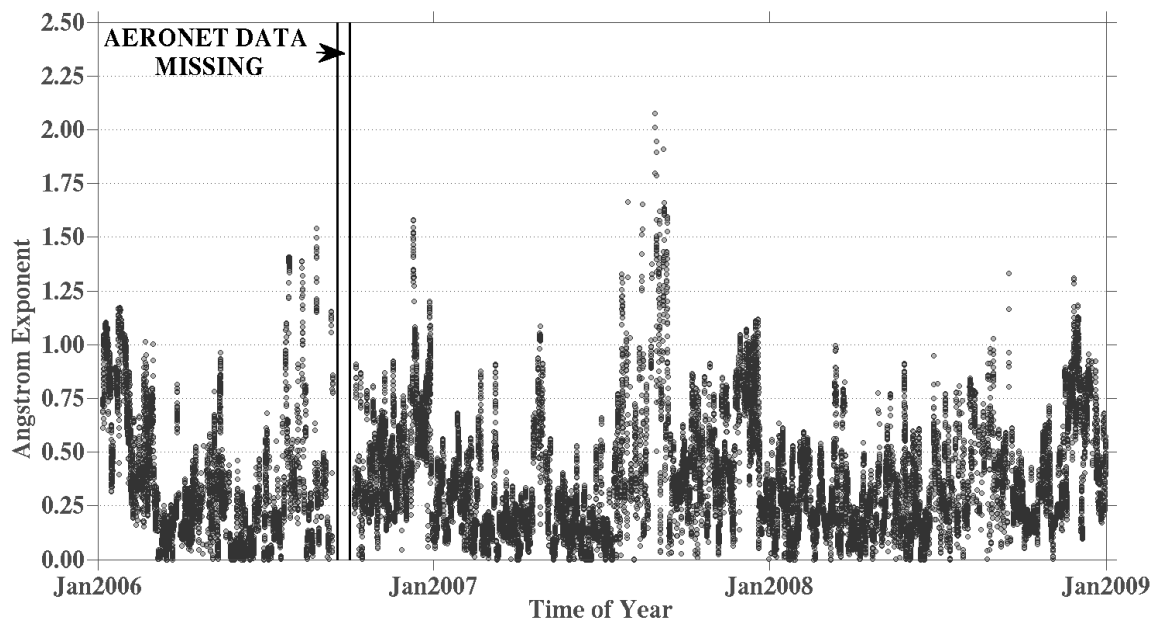
Figure 7. Time series plot of the Angstrom Exponent at the IER Cinzana AERONET site. All available 675 nm and 440 nm Level 2.0 data is used in calculating the Angstrom Exponent. Measurements are conducted every 15 minutes.
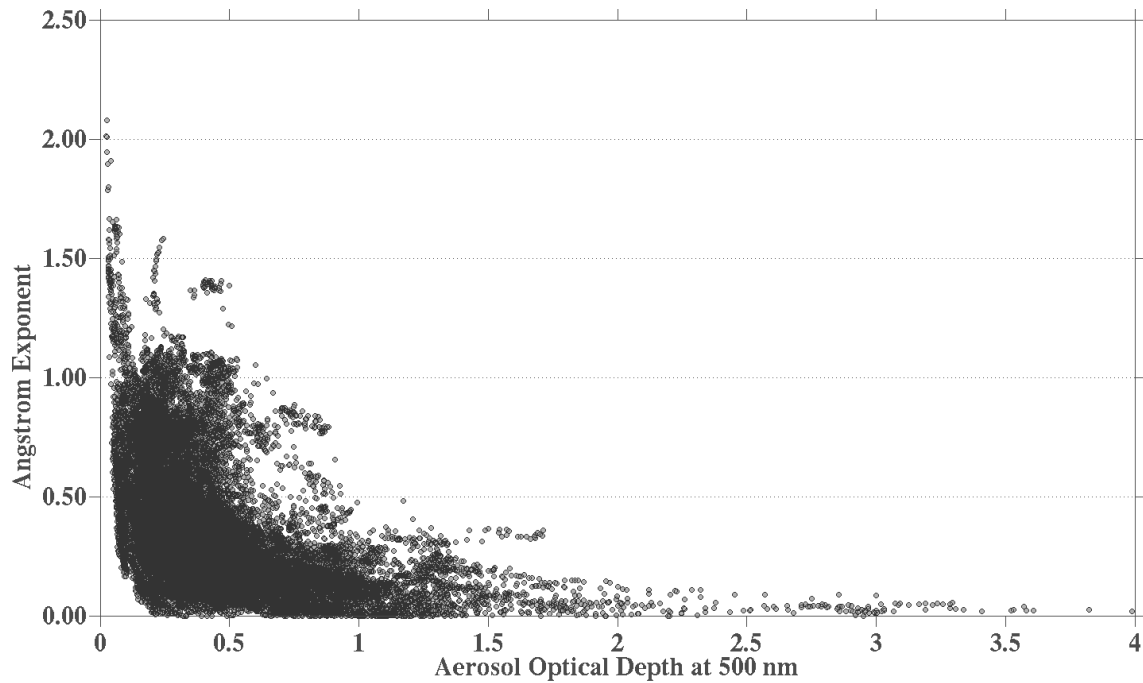
Figure 8. Scatter plot of level 2.0 data from the IER Cinzana AERONET site from the beginning of 2006 to the end of 2008. Measurements are conducted every 15 minutes.

Figures 9 through 14 show that during the rainy season in Mali the early afternoon aerosol burden (noon-2 pm AOD average) experiences day-to-day variability. Daily aerosol burden variability is likely due to shifting long-range source regions or changes in local loading dependent on frequency of precipitation events. Typically, there are more days with lower AE in the drier months (June and October) than in wetter months (Figs. 10). More days with lower AE indicates that aerosols from dust source regions are more prevalent during the dry season. The aerosol variability in 2007 (Fig. 11) is similar to 2006 (Fig 9), except there are four days in June with AOD greater than the maximum AOD in 2006 of 1.5. Figs. 9 through 14 show that there are days during the rainy season that have higher AE and higher AOD which likely have higher CCN concentrations. Therefore, project personnel in Mali can use AERONET observations to plan on conducting hygroscopic cloud seeding flights when the AOD and AE are higher.

24
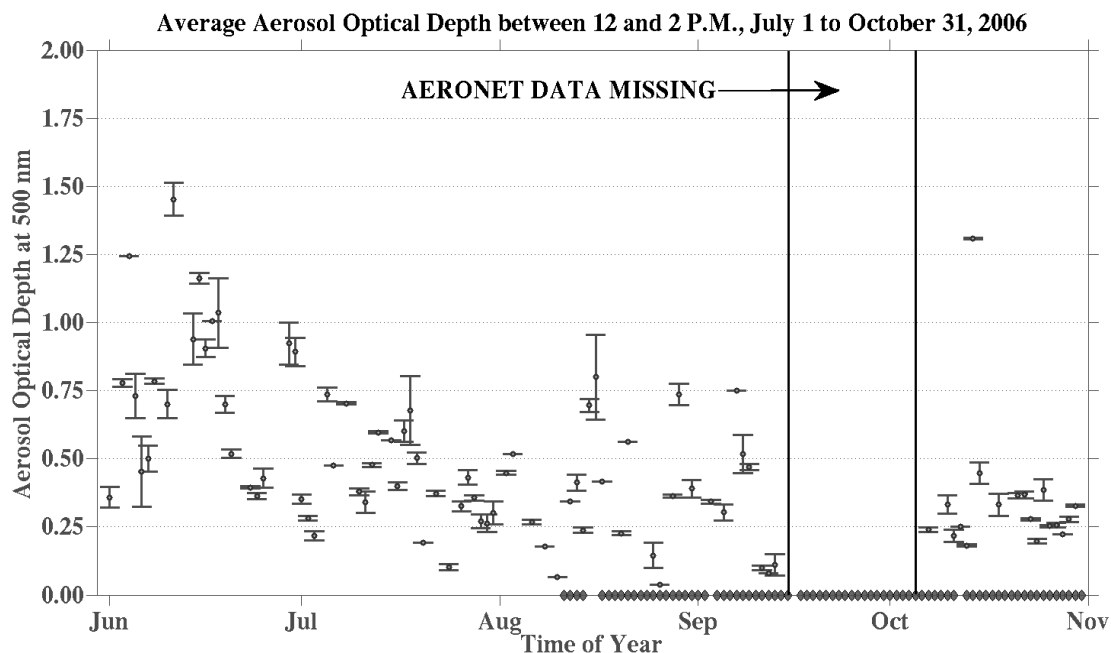
Figure 9. Noon to 2 pm local time average (solid circles) and one standard deviation (vertical lines) of the Aerosol Optical Depth (AOD) at 500 nm for all Level 2.0 data from the IER Cinzana AERONET site are plotted for 2006. The diamonds along the x-axis denote days when radar data is available from the Bamako, Mali site.
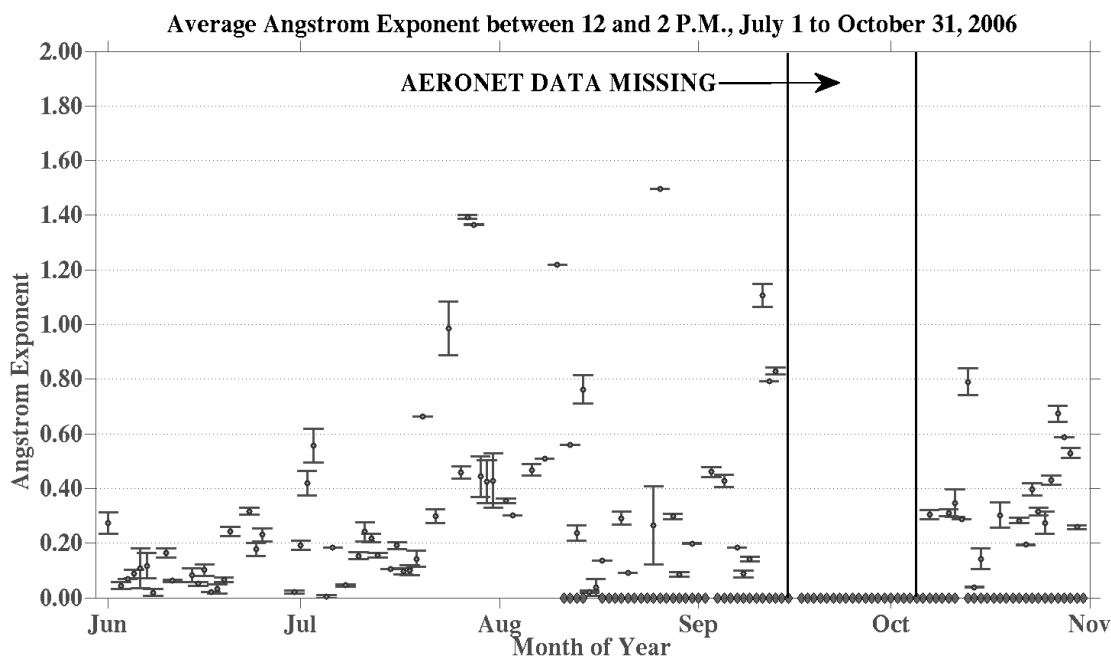
Figure 10. Same as Fig. 9 except the variable of interest is Angstrom Exponent (440/675 nm).

25
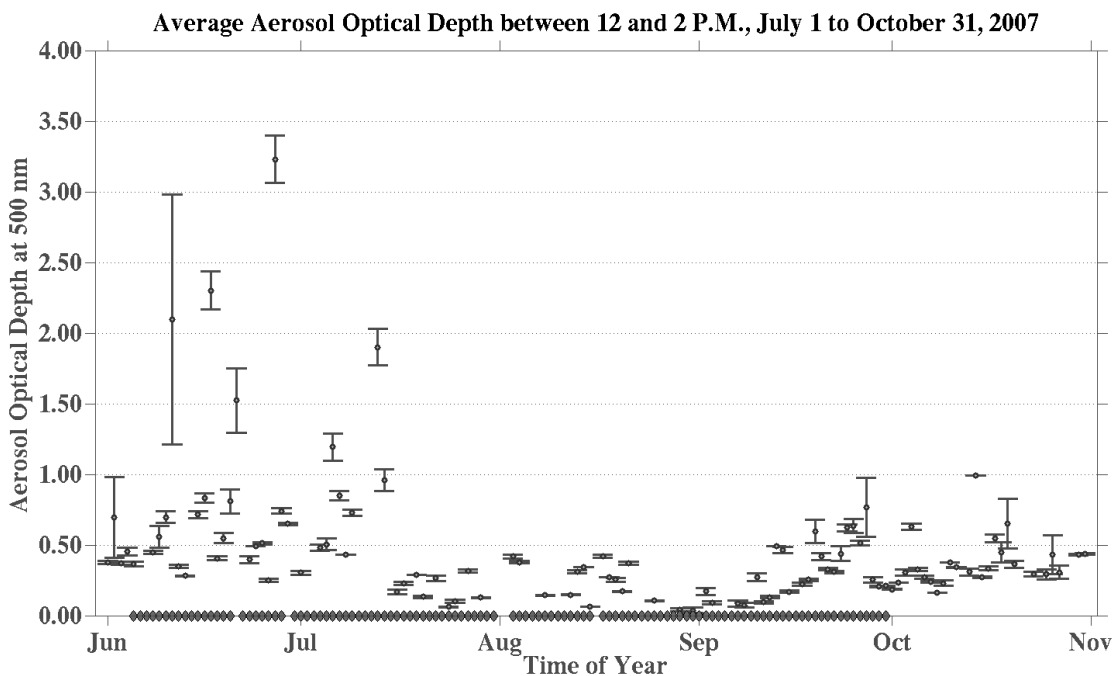
Figure 11. Same as Fig. 9 except period of interest is June 1 to October 31, 2007.
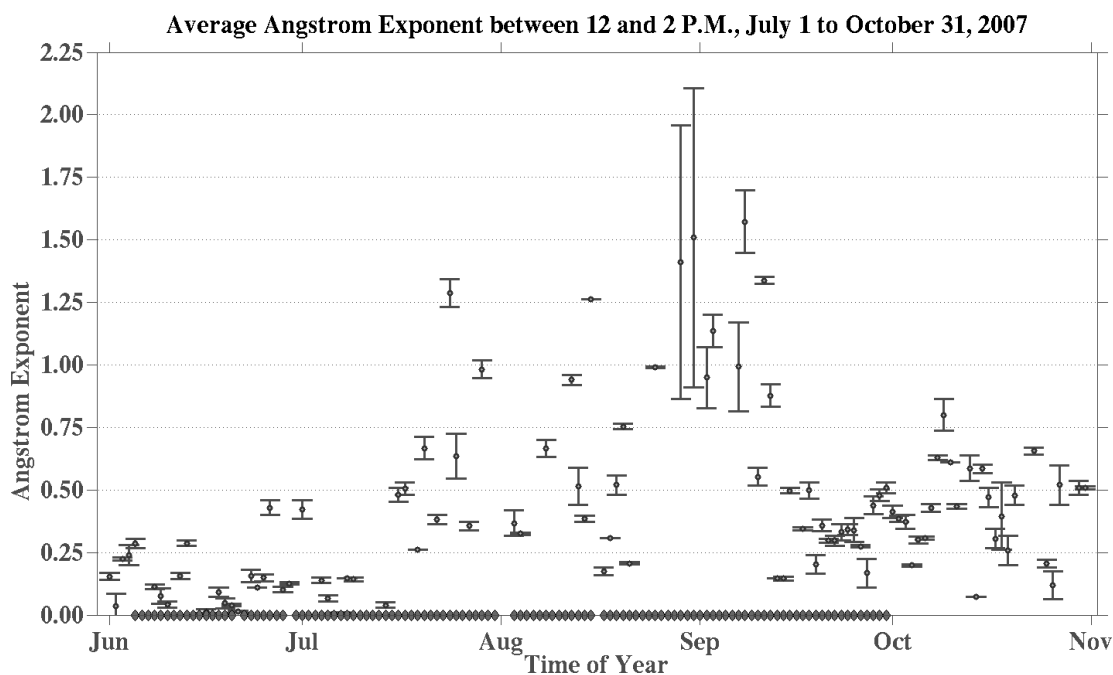
Figure 12. Same as Fig. 11 except variable of interest is Angstrom Exponent (440/675 nm).
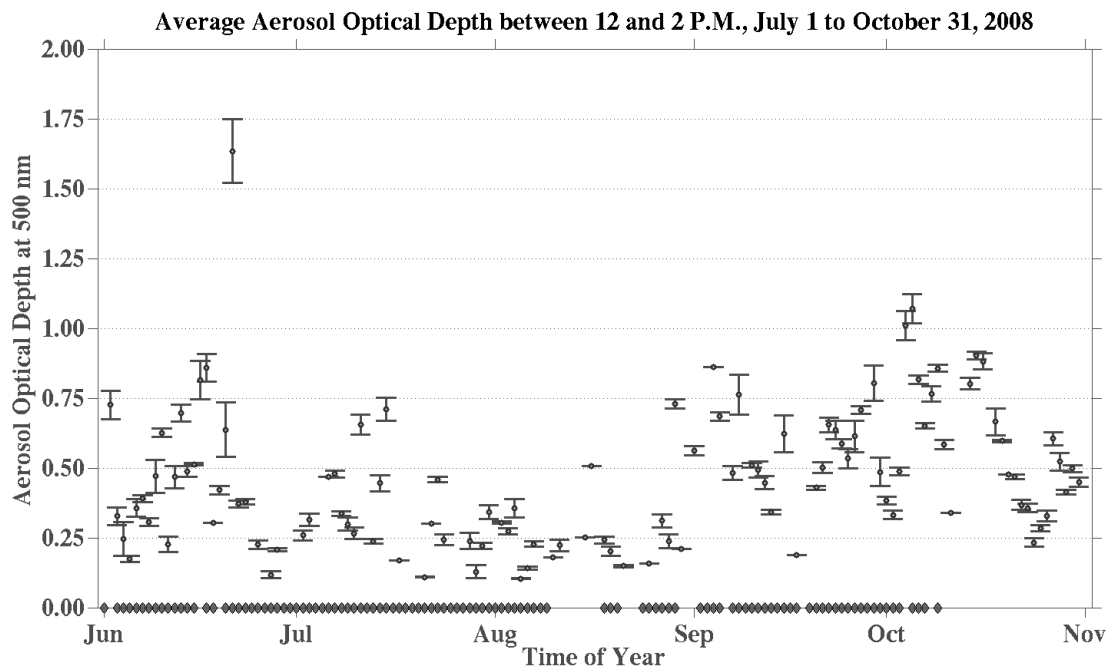
Figure 13. Same as Fig. 9 except period of interest is June 1 to October 31, 2008.
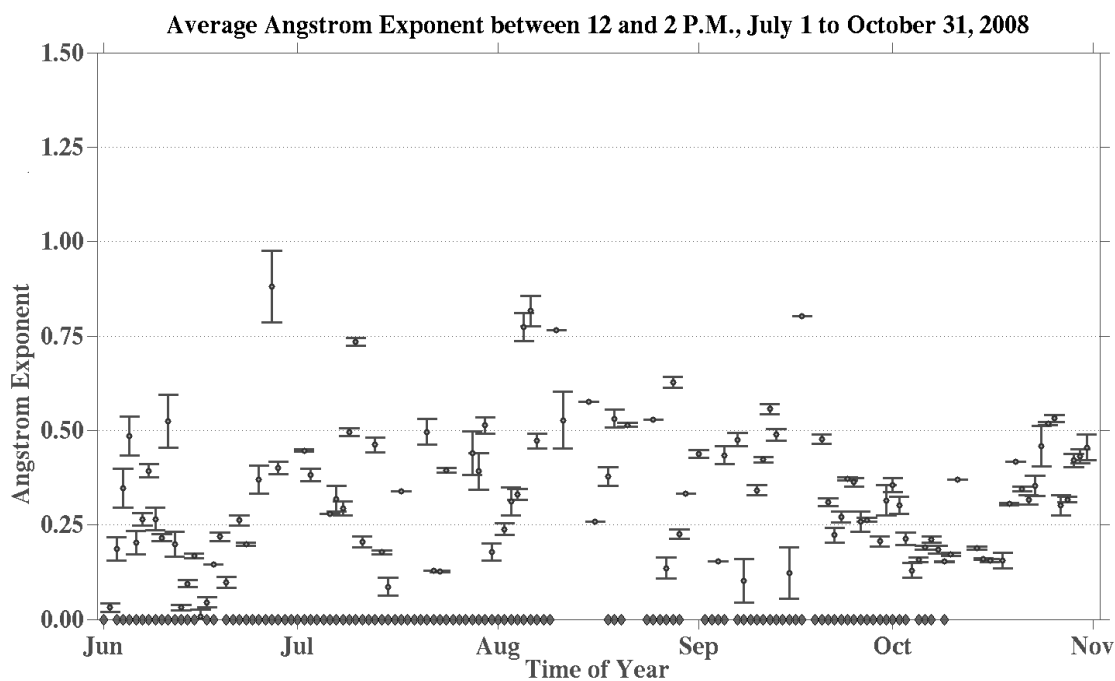
Figure 14. Same as Fig. 13 except variable of interest is Angstrom Exponent (440/675 nm).

27

Data Filtering by Angstrom Exponent, Convective Available Potential Energy, Lifting Condensation Level and Shear

Figures 15 through 26 show the results of applying AE and balloon sounding parameter filtering. Filtering removes days from the analysis dataset based on AE, CAPE, LCL and shear thresholds. Comparing Figs. 15 and 16 shows that removing days with AE less than or equal to 0.35 necessarily also has the effect of removing days with larger AOD. The AE threshold filter removes a total of twenty-five hundred cells. The AE filter removes 11 days (240 cells) for AOD 0.2 to 0.3, 27 days 600 cells) for AOD 0.3 to 0.4, 22 days (650 cells) for AOD 0.4 to 0.5, 11 days (180 cells) for AOD 0.5 to 0.6, 12 days (180 cells) for AOD 0.6 to 0.7 and 18 days (450 Cells) for AOD 0.7 to 1.0.
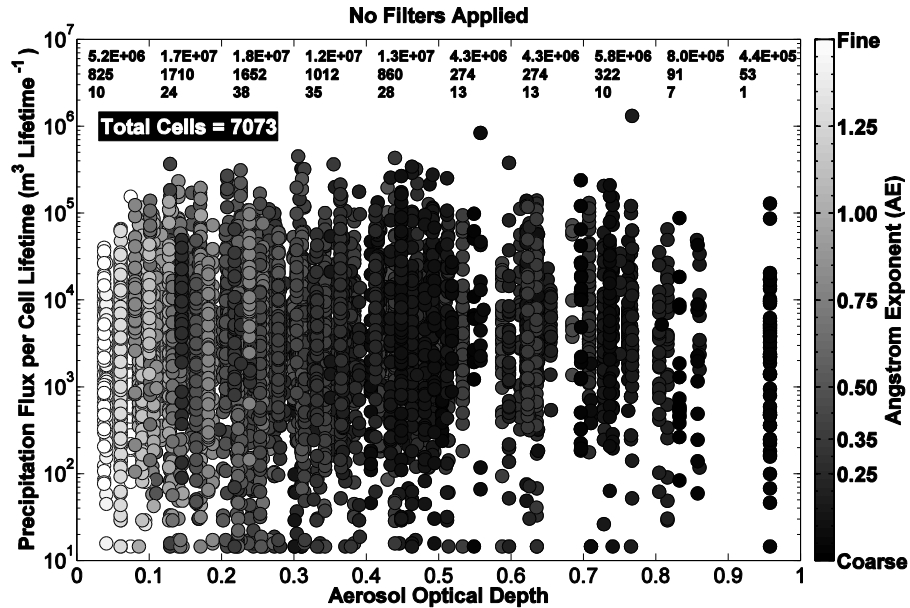
Figure 15. Cell Precipitation Flux sum for the cell's lifetime plotted as a function of Aerosol Optical Depth (AOD). AOD at 500 nm is calculated by averaging measurements obtained between 1200 and 1400 local time. Each point is shaded in gray scale according to its day's respective average Angstrom Exponent (AE) (440/675 nm) for 1200 to 1400 local time. Sum totals of precipitation flux, cells and days for each bin are printed across the top of the plot area. Precipitation flux, storm cells, and number of days represented in each bin are presented from top to bottom, respectively. The sum of all the cells plotted is printed in the black background Total Cells box. The x-axis range is limited to 0.0 through 1.0; however, there are eight days of data with AOD greater than 1.0. These eight days are now shown here because they are removed later by the AE filter.
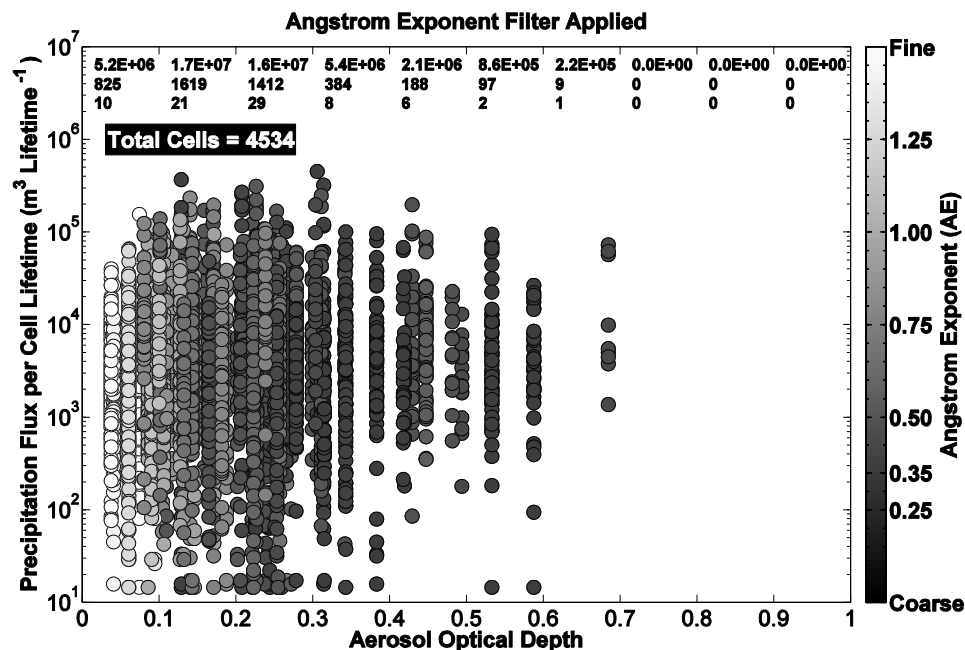
Figure 16. Same as Fig. 15 except only days with means AE (440/675 nm) greater than 0.35 are included.
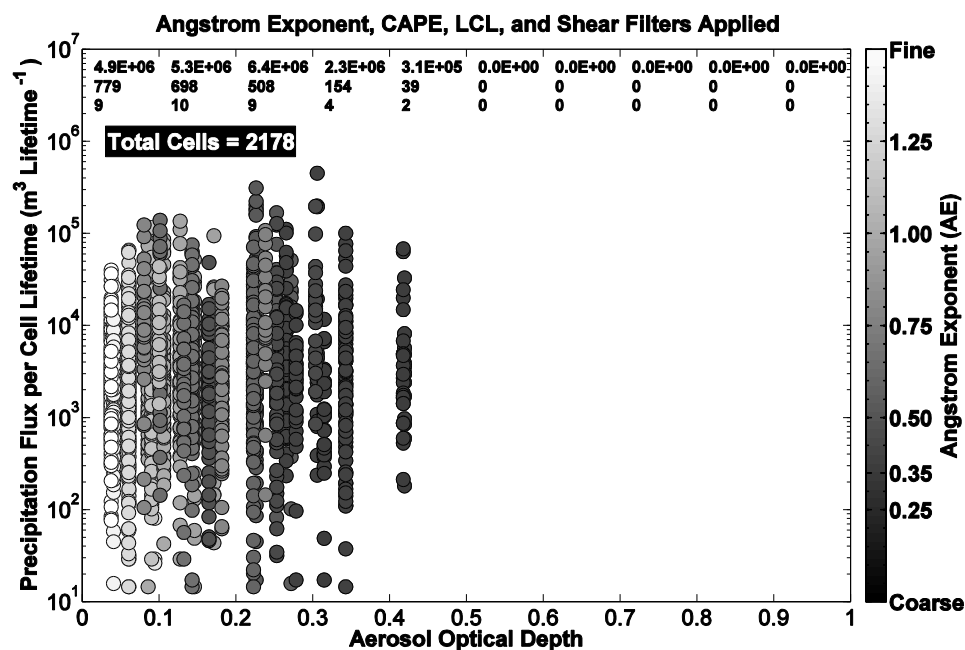
Figure 17. Same as Fig. 15 except that only days with AE (440/675 nm) greater than 0.35, CAPE greater than 1000 J Kg^{-1}, LCL less than or equal to 2.5 Km AGL and wind shear less than 30 m s^{-1} are included.
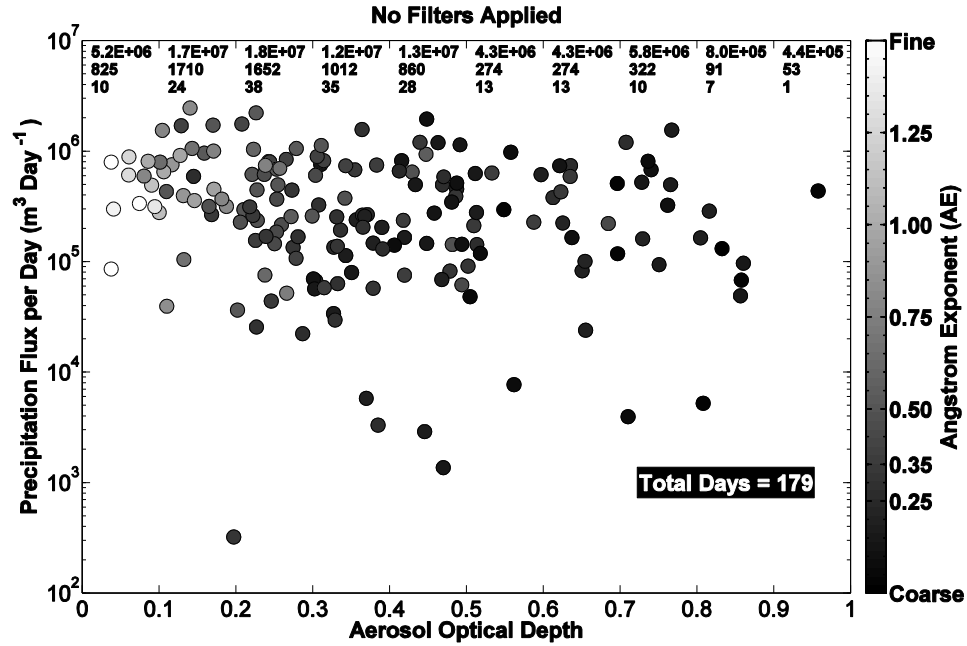
Figure 18. Same as Fig. 15 except that the total precipitation flux for a day is plotted instead of the precipitation flux per cell.
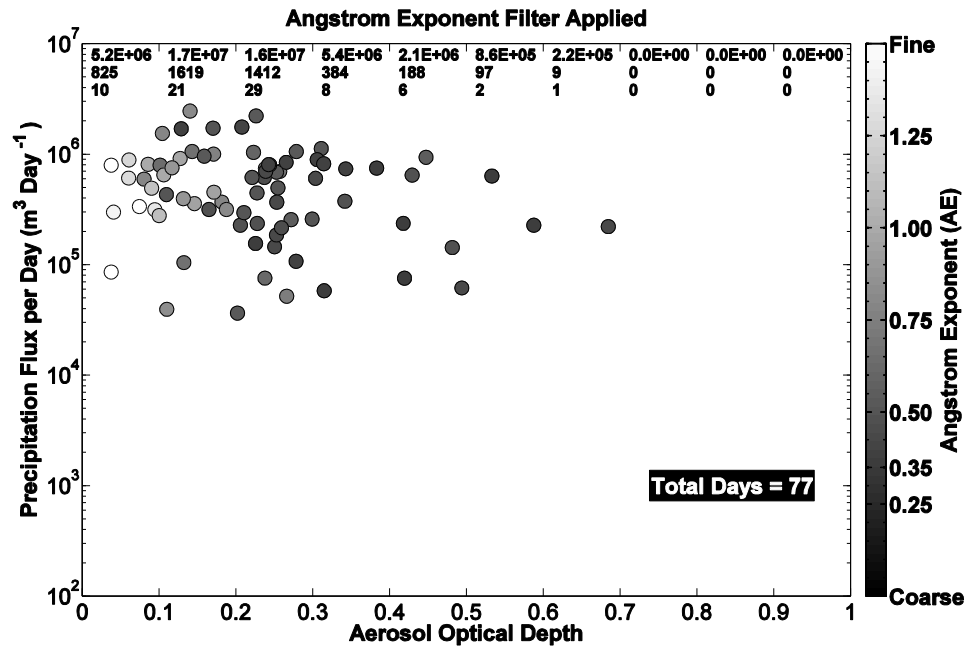
Figure 19. Same as Fig. 15 except that the total precipitation flux for a day is plotted instead of the precipitation flux per cell and only days with AE (440/675 nm) greater than 0.35 are included.
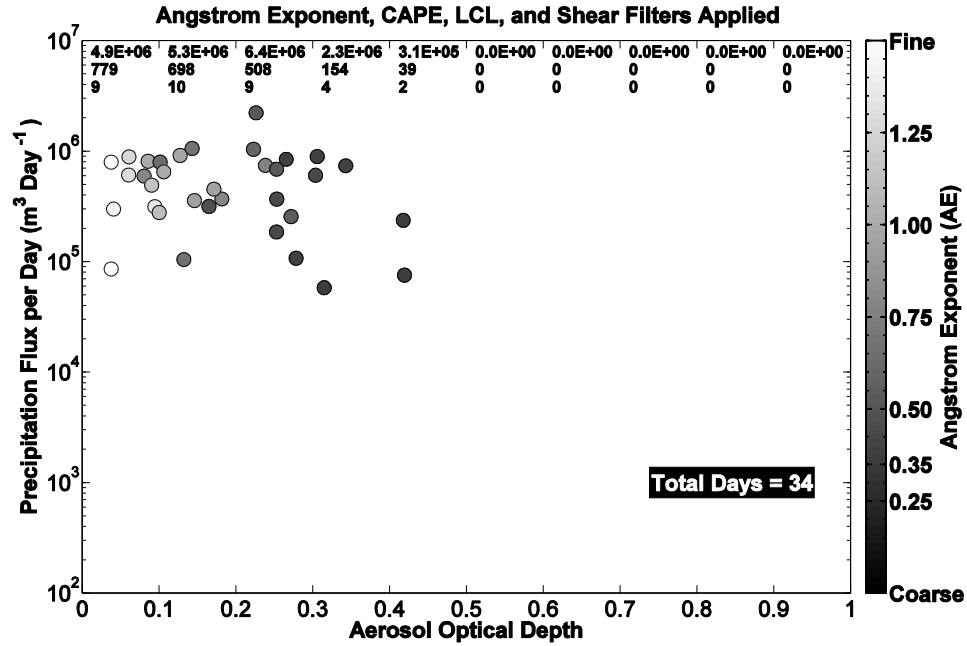
Figure 20. Same as Fig. 15 except that the total precipitation flux for a day is plotted instead of the precipitation flux per cell, only days with AE (440/675 nm) greater than 0.35, CAPE greater than 1000 J Kg^{-1}, LCL less than or equal to 2.5 Km AGL and wind shear less than 30 m s^{-1} are included.
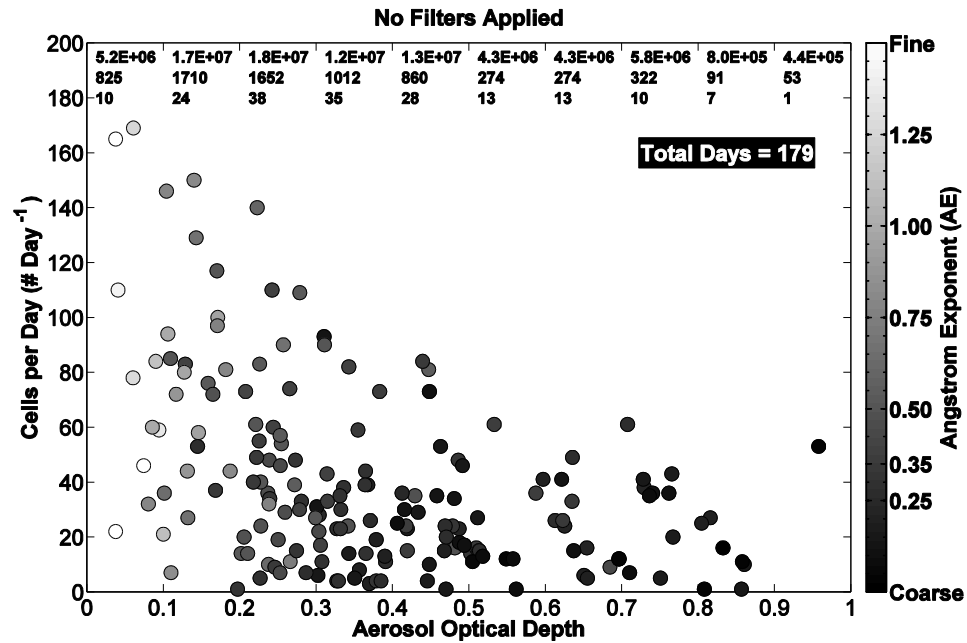
Figure 21. Same as Fig. 15 except that the number of cells per day is plotted instead of precipitation flux per cell.
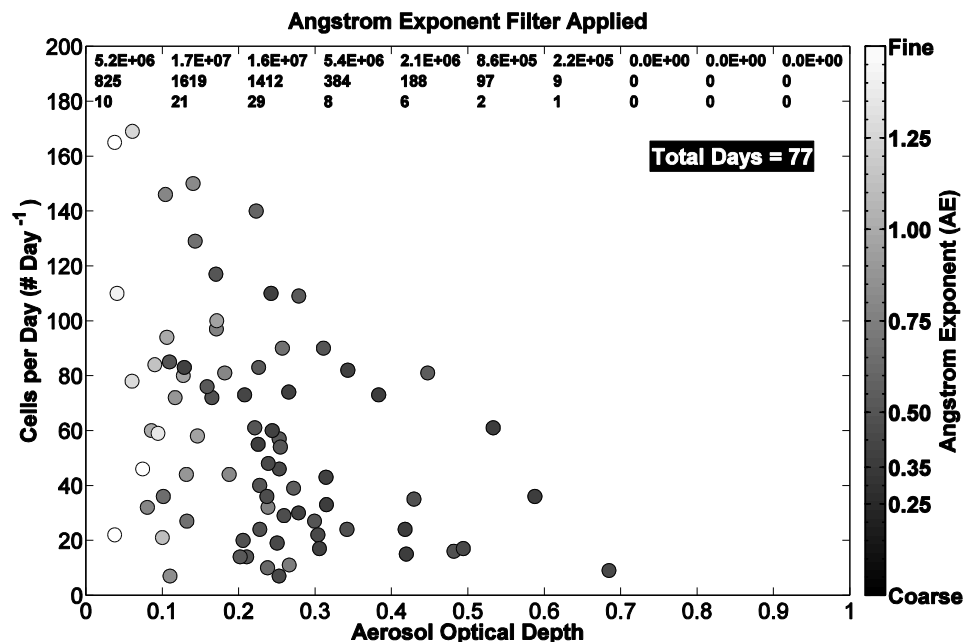
Figure 22. Same as Fig. 15 except that the number of cells per day is plotted instead of precipitation flux per cell, and only days with AE (440/675 nm) greater than 0.35 are included.
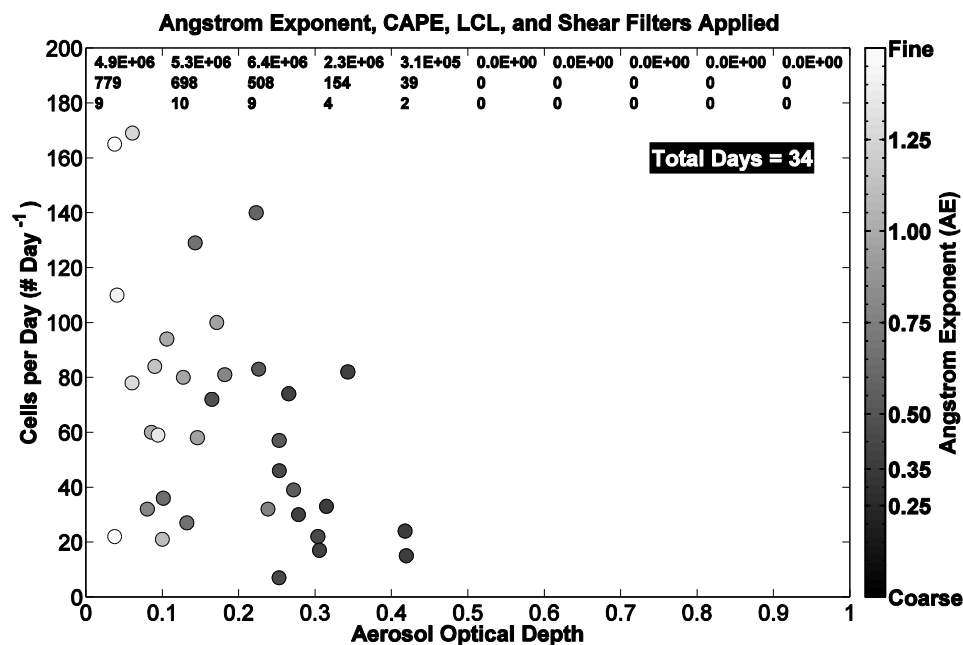
Figure 23. Same as Fig. 15 except that the number of cells for a day is plotted instead of the precipitation flux per cell, only days with AE (440/675 nm) greater than 0.35, CAPE greater than 1000 J Kg^{-1}, LCL less than or equal to 2.5 Km AGL and wind shear less than 30 m s^{-1} are included.

No Filters Applied

2.2E+04	4.4E+04	4.4E+04	2.7E+04	2.3E+04	7.4E+03	7.7E+03	8.6E+03	2.6E+03	1.2E+03
825	1710	1652	1012	860	274	274	322	91	53
10	24	38	35	28	13	13	10	7	1

Total Cells = 7073
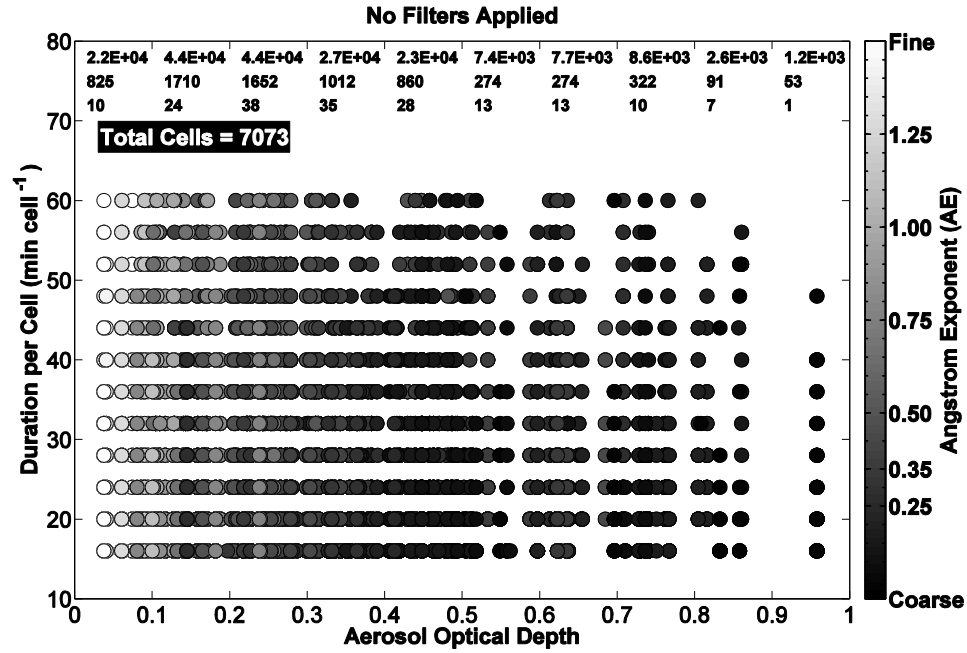
Figure 24. Same as Fig. 15 except that the duration of a cell's lifetime is plotted instead of precipitation flux per cell.

Angstrom Exponent Filter Applied

2.2E+04	4.2E+04	3.8E+04	1.0E+04	5.3E+03	2.7E+03	2.8E+02	0.0E+00	0.0E+00	0.0E+00
825	1619	1412	384	188	97	9	0	0	0
10	21	29	8	6	2	1	0	0	0

Total Cells = 4534
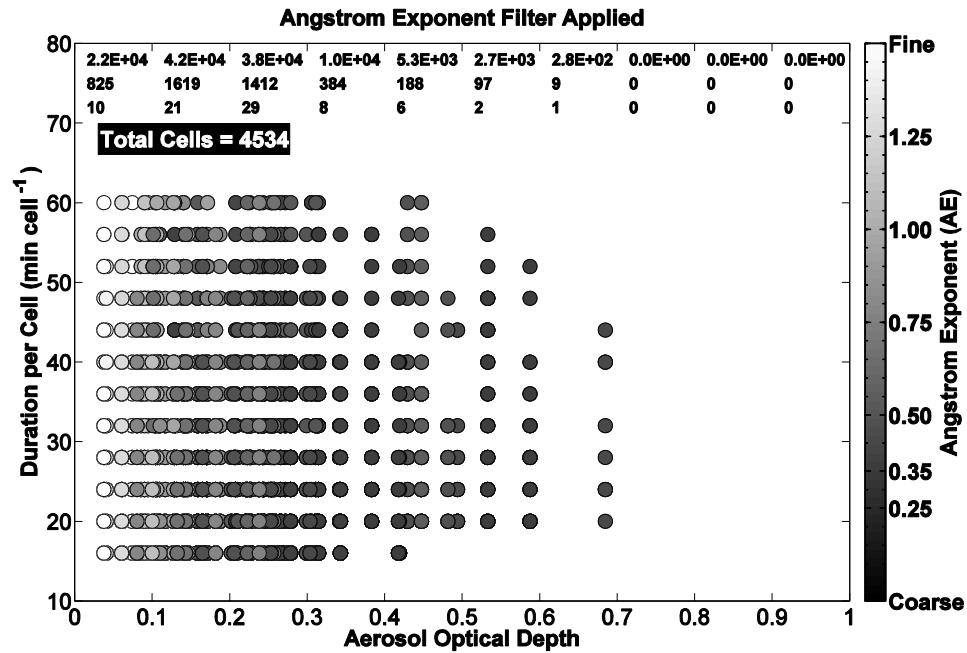
Figure 25. Same as Fig. 15 except that the duration of a cell's lifetime is plotted instead of precipitation flux per cell, and only days with AE (440/675 nm) greater than 0.35 are included.

33

Angstrom Exponent, CAPE, LCL, and Shear Filters Applied

2.1E+04	1.7E+04	1.3E+04	4.1E+03	9.5E+02	0.0E+00	0.0E+00	0.0E+00	0.0E+00	0.0E+00
779	698	508	154	39	0	0	0	0	0
9	10	9	4	2	0	0	0	0	0

Total Cells = 2178

Y-axis: Duration per Cell (min cell^{-1}) — 10, 20, 30, 40, 50, 60, 70, 80

X-axis: Aerosol Optical Depth — 0, 0.1, 0.2, 0.3, 0.4, 0.5, 0.6, 0.7, 0.8, 0.9, 1

Color bar (right): Angstrom Exponent (AE) — Fine (top), 1.25, 1.00, 0.75, 0.50, 0.35, 0.25, Coarse (bottom)
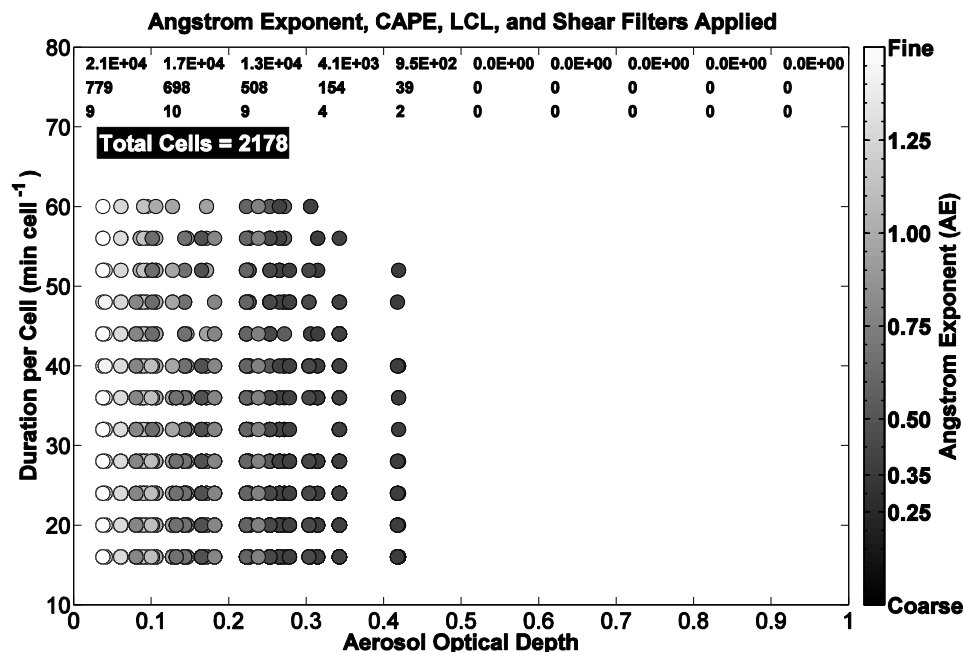
Figure 26. Same as Fig. 15 except that the duration of a cell is plotted instead of the precipitation flux per cell, only days with AE (440/675 nm) greater than 0.35, CAPE greater than 1000 J Kg^{-1}, LCL less than or equal to 2.5 Km AGL and wind shear less than 30 m s^{-1} are included.

Cells are assumed to be convective single cells that initiated in similar thermodynamic and dynamic environments with similar boundary layer moisture profiles that did not merge with other cells or split into more cells. Days where CAPE is less than 1000 (J kg^{-1}), shear greater than 30 m s^{-1} and Lifting Condensation Level (LCL) greater than 2.5 km AGL are removed from the analyzed data set. Results of these filters on precipitation flux per cell, duration per cell, precipitation flux per day and cells per day are shown in Figs 17, 20, 23 and 26, respectively. The filters removed ~2400 cells primarily due to missing sounding data; only 47 cells are removed due to insufficient CAPE and no cells are removed due to the shear and LCL thresholds. The reduction in cell numbers is primarily due to missing sounding data or the necessary data not being available to perform a calculation. Unavailable data could occur because entries, such as

temperature, in a raw sounding file are flagged as poor quality. Too many flags for poor quality temperature may prevent calculating for CAPE and LCL. Shear calculations are not possible if wind data is missing in the levels between 5.5 and 6.5 and 0.0 and 1.0 (km AGL). CAPE, shear, and LCL filters remove 404, 54 and 430 cells, respectively, because flagged radiosonde data produces null results for calculations of these variables. The number of cells removed because no atmospheric sounding is available on their corresponding day numbered 1692. In the end, the cells are removed mostly because of poor data quality or availability issues and not because of the applied CAPE, LCL, and shear filters' thresholds; however, the filtering ensures that a similar thermodynamic and dynamic environment is reasonably assured to exist across all of the days analyzed.

Figure 27 depicts the thirty-four days that passed all of the filters. Only two days in 2008 pass to the analysis stage because of unavailable atmospheric sounding data from June 15 to October 27, 2008. Unavailable radar data during June and July 2006 explains the data gap present in Fig. 27. The lack of data for June and October 2007 (Fig. 27) occurs because of missing radiosonde, AERONET or radar data. Missing AERONET data during the 12:00 to 14:00 time frame or missing radar data during the 13:00 to 21:00 time frame would eliminate days from the analysis.
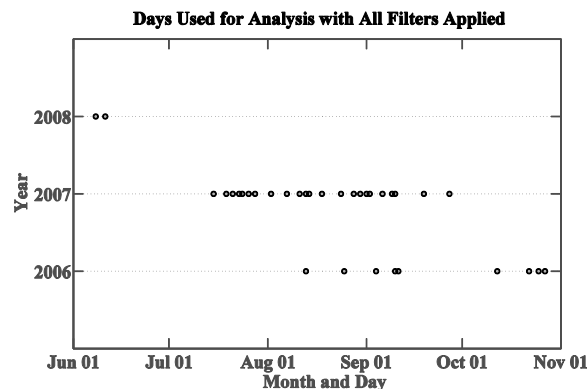
Figure 27. The days that remain after the CAPE, LCL and shear filters are applied.

35

Correlations between Aerosol Robotic Network Stations

The IER Cinzana AERONET station is the closest site to the Bamako radar facility for 2006, 2007 and 2008 period. Wind at Bamako on 20 of 34 days is from the east and southeast (Fig. 28), and IER Cinzana is located 240 km to the northeast of the city. Therefore, the possibility exists that IER Cinzana does not sample the air mass that propagates over the Bamako radar domain between 12:00 through 14:00 local time. The following question is addressed after completing the correlation analysis: "Is distance or being upwind more important to obtaining an accurate air mass representation over Bamako?"
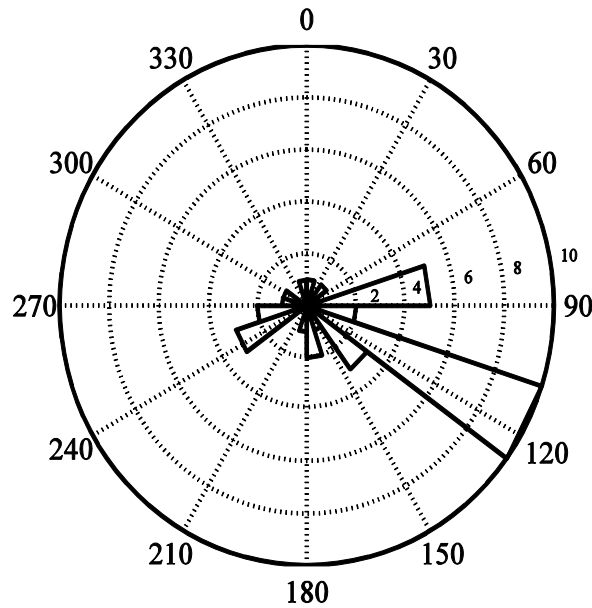
Figure 28. Frequency of wind direction calculated from Bamako soundings at 12:00 local time. The wind direction is an average from 0 to 3 km AGL wind data. Envelopes in bold highlight the azimuth envelop for the direction the wind came from for the 34 days presented in Fig. 27. The numbers between 60 and 90 °, leading from the center outward, indicate the number of days that a respective wind direction occurred.

IER Cinzana is compared to three stations listed in Table 2 by calculating correlation coefficients (Table 2) for average AOD from the period 12:00 through 14:00. The Ouagadougou station achieved the highest correlation coefficient of 0.78 with IER

36

Cinzana, which is impressive considering that the separation between the stations is 505 km (Table 2). The Banizoumbou station achieved the lowest correlation coefficient of 0.31 with IER Cinzana, which is located 940 km to the east. Ouagadougou achieves a correlation of 0.78 and is closer than Banizoumbou to IER Cinzana. One can conclude that the correlation between two stations' AOD data sets improves by decreasing their separation distance; however, Ouagadougou and Agoufou achieve different correlation coefficients of 0.47 and 0.78 and are located roughly the same distance from IER Cinzanza. Agoufou is located to the northeast and Ouagadougou to the southeast, indicating that wind direction is more important to influencing AOD over a region than distance (Table 2) and climate region (Fig. 2). Therefore, the optimal location for an AERONET station is to the southeast and closer to the Bamako radar; however, Ouagadougou is not used for this study because there are no data available during 2008.

Table 2. Correlation, distance and direction between AERONET station IER Cinzana and stations Agoufou, Banizoumbou and Ouagadougou. Correlation coefficients are calculated using the time frame June 8 through October 28, in 2006, 2007 and 2008, for Agoufou and Banizoumbou, and in 2006 and 2007 for Ouagadougou.

	IER Cinzana (13 °N 5 °W)		
	Correlation	Distance (km)	Direction
Agoufou (15 °N 1 °W)	0.47	520	NE
Banizoumbou (13 °N 2 °E)	0.31	930	E
Ouagadougou (12 °N 1 °W)	0.78	505	SE

Linear Least Squares Fit Lines

Simple convective cells filtered for dust and surface based sounding parameters are used to assess the relationship between increasing AOD and radar derived precipitation in Mali, West Africa. Linear regression is computed for the median precipitation flux per cell (Fig. 29), precipitation flux summed over all the cells on a respective day (Fig. 30), median duration per cell (Fig. 31) and cells per day (Fig. 32).

The MATLAB software package function, regstats, is used to compute the regression fit lines and their statistics. R^2, slope and p-value are computed for each fit line and results can be found in Table 3. The R^2 is the amount of change in y that can be attributed to the change in x. R^2 of 0.01, 0.05 and 0.05 indicates that one, five and five percent of the change in median precipitation flux per cell, duration per cell and flux per day, respectively, is attributable to the change in AOD. To obtain the p-values, regstats calculates a t-statistic for the slope and compares it to the Student's t-distribution. The p-value is the probability of witnessing a result as extreme as the fit lines obtain in Figs. 29 through 32 in a collection of random data. The following question is answered by the p-value: "If there is no linear relationship between x and y overall, what is the probability that randomly selected points result in a regression line as far from the horizontal, or further, than was originally observed?" The null hypothesis is that no relationship exists between AOD and the respective y-axis parameter and their true correlation is zero. The level of significance is set to the generally accepted confidence level 95 % (p-value = 0.05), and the null hypothesis is rejected when the p-value for a fit line is less than 0.05; however, statistical significance is tested on four relationships. Therefore, to be more statistically robust and account for multiplicity using the Bonferroni method (Bender and Lange 2000; Bland and Altman 1995), the level of significance is set to a confidence level of 98.75 % (p-value = 0.0125). With a p-value less than or equal to 0.0125, there is a 5 % chance that at least one of the lines in Figs. 29 through 32 would have occurred in a random sample where no real relationship exists. Therefore, a p-value less than 0.0125 would indicate a relationship is significant at the 95 % confidence level.
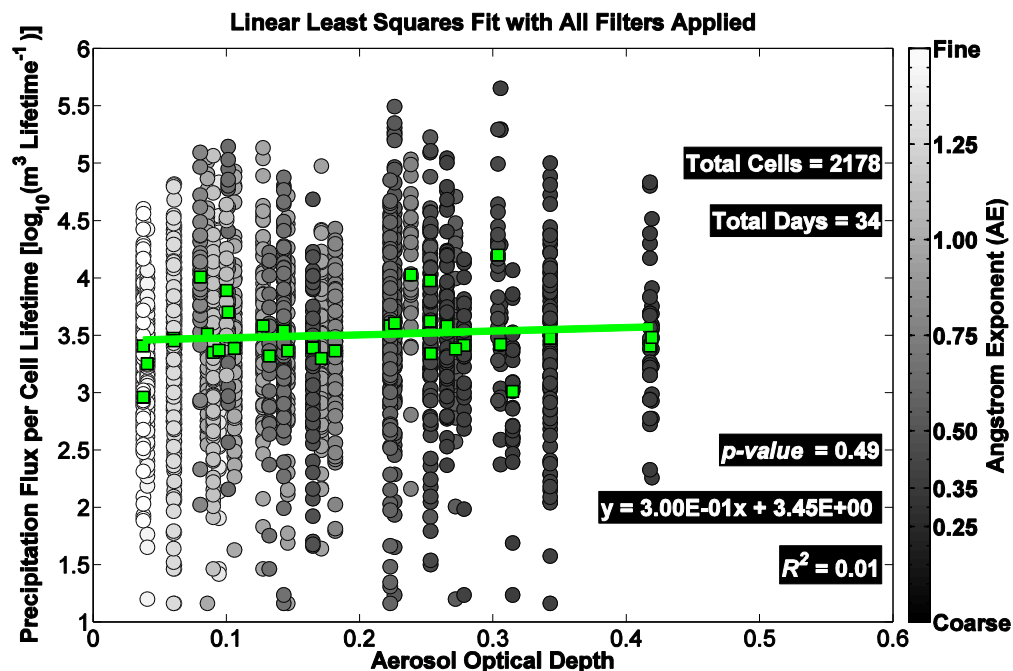
Figure 29. Plot of the pairings of the sum of precipitation flux for a cell and averaged 12:00 to 14:00 local time AOD that occurred on the same day. The green boxes are the daily median precipitation flux per cell; green line is the linear regression fit to the medians; slope, p-value and R^2 are printed on the right; slope is in logarithmic units.
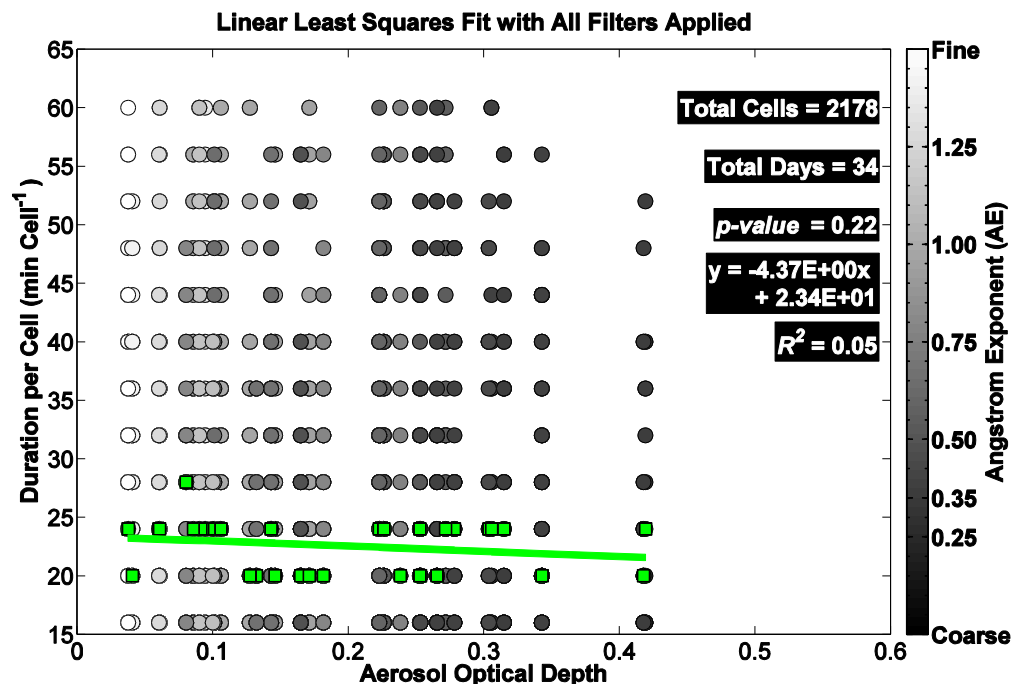
Figure 30. Plot of the pairings between duration of a cell's life and that storm day's AOD (shaded by AE (440/675 nm)). The remainder of this plot is explained by the caption for Fig. 29.
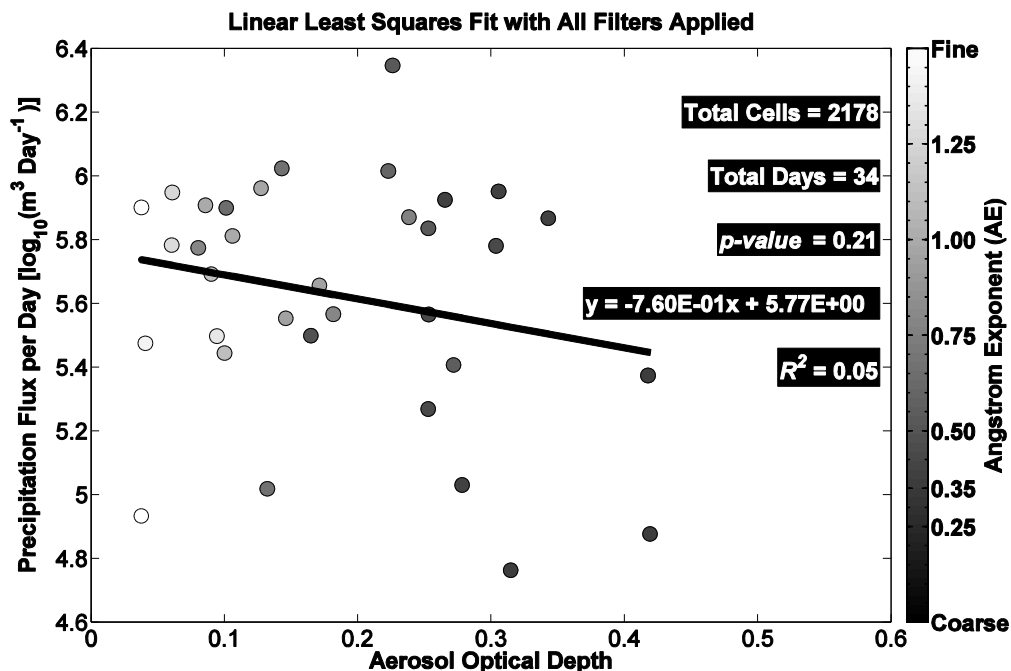
Figure 31. Plot of the sum total of all the simple cells' precipitation fluxes that occur for a day as a function of that day's AOD. Slope printed on this plot is in logarithmic units. The remainder of this plot is explained by the caption for Fig. 29.
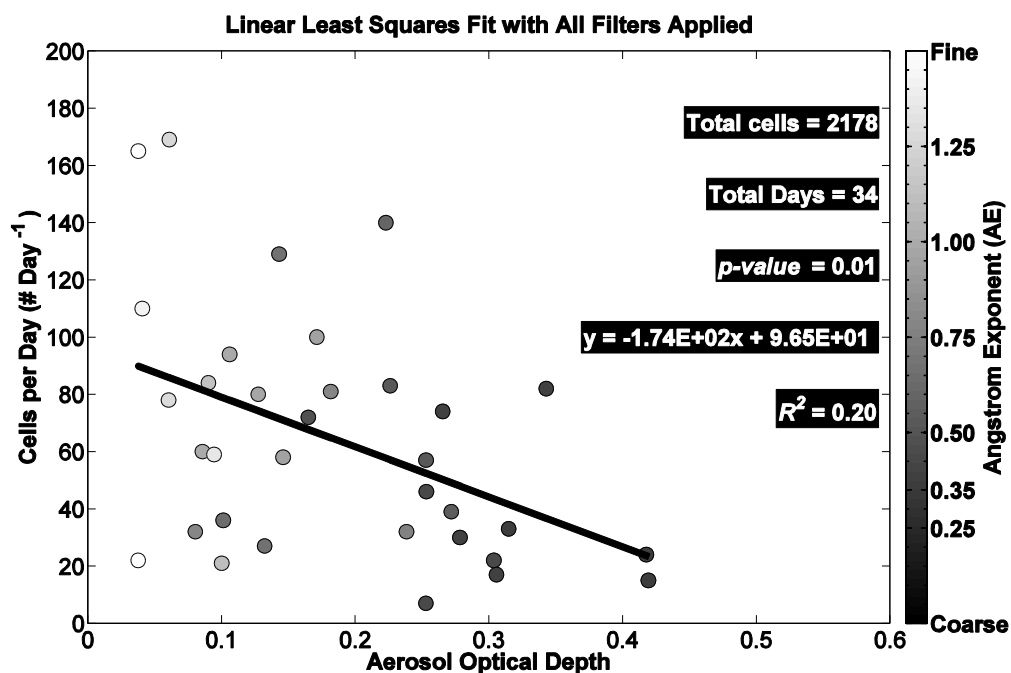
Figure 32. Plot of the sum total of cells for a respective day paired with the AOD on that day. The slope printed on this plot is shown in linear units. The remainder of this plot is explained by the caption for Fig. 29.

Table 3. Shows results of slope, t-statistic and p-value for each slope, and R^2 calculations computed for Figs. 29 to 32's regression lines. R^2 is the coefficient of determination. Slopes for Flux per Cell and Flux per day are in logarithmic units as displayed in Figs. 29 and 31, and Dur. per Cell (Duration per Cell) and Cells per Day are in linear units as shown in Figs. 30 and 32.

	Slope	t-statistic	p-value	Significant	R^2
Flux per Cell	0.30	-1.28	0.492	No	0.01
Dur. per Cell	-4.37	0.69	0.218	No	0.05
Flux per Day	-7.60	-2.79	0.211	No	0.05
Cells per Day	-174.0	-1.26	0.009	Yes	0.20

The regression lines presented in Figs. 29, 30 and 31 seem to indicate an increase in precipitation flux per cell, and decrease in duration per cell and flux per day as AOD increases. However, the p-values of 0.492, 0.218 and 0.211 indicate that the null hypothesis is not rejected for the relationships: AOD-Precipitation Flux per Cell (Fig. 29), AOD-Duration per Cell (Fig. 30) and AOD-Flux per Day (Fig. 31). In other words, there is a greater than 5 % probability that the fit lines occurred by chance. Outlier points that could affect the linear regression fits are evident in Figs. 29 and 31. In Fig. 29 there are five outlier points above the fit line equal to four log units, approximately, and two outlier points below the fit line equal to three long units, approximately. In Fig. 31 there are four points below 5.2 and one point above 6.2 log units. After an in-depth review of the data, the outlier days do not appear to suffer from any issues related to the radar's operation or software processing. For the days with higher precipitation flux there is a greater proportion of larger cells, and for the days with lower precipitation flux there is a lesser proportion of larger cells. Therefore, the non-significant (Figs. 29 through 31) relationships are valid with respect to data quality.

AOD-Cells per Day (Fig. 32) is the only significant relationship. The total number of cells per day is shown in Fig. 32 where each point represents the total number

of cells tracked between the hours of 13:00 and 21:00 local time. Radar data are inspected for outlier points. Very high cell numbers are a result of days that experience scattered unorganized convection, and days with low cell numbers show limited cell activity or a combination of organized and unorganized convection. The two points with AOD greater than 0.4 (Fig. 32) are from days with limited cell activity. The p-value of 0.009 (Table 3) computed for the regression line of Fig. 32 (cells per day) indicates a statistically significant (p-value < 0.0125) negative slope (Table 3). Therefore, the regression line did not likely occur by chance, and days with higher AODs experience fewer cells. R^2 equal to 0.20 indicates a poor linear relationship between AOD and number of cells per day. Therefore, it is not appropriate to use the regression line as a cell total per day, "prediction," scheme; however, 20 % of the decrease in cells per day is attributable to the increase in AOD. Attributing 20 % of the decrease in cells per day to the increase in AOD is impressive considering the complexity of precipitation formation processes.

CHAPTER V

CONCLUSIONS AND FUTURE WORK

Bamako, Mali radar data from 2006, 2007 and 2008 are compared to AOD data obtained from an AERONET site located 240 km to the northeast. AOD is chosen as the variable to represent the concentration of aerosols that could influence microphysical processes responsible for cloud and precipitation development. The following assumptions are made: 1) the majority of aerosols are concentrated in the boundary layer of the atmosphere and 2) increasing AOD infers an increasing concentration of CCN for a region clear of desert dust particles. To increase the likelihood that cells analyzed are of the simple convective type, and AOD is not desert-dust-contaminated, filters are applied based on CAPE, shear, LCL and AE.

The objective is to determine whether increasing AOD has a negative influence on radar derived precipitation. There relationships: AOD-Precipitation Flux per Cell, AOD-Cell Duration and AOD-Precipitation Flux per Day are not significant. However, the AOD-Cells per Day relationship is significant with p-value and R^2 equal to 0.009 and 0.20, respectively. Simple cells per day decreasing with increasing AOD indicates that clouds are inhibited from producing precipitation size droplets large enough to produce energy returns detectable by Mali's C-band radar. The inverse linear relationship found between AOD and cells-per-day seems to be positive confirmation of the second indirect effect. Part of Rosenfeld (2008) is confirmed with respect to increasing concentrations of

smaller size particles, resulting in smaller effective radii and reduced collisions and coalescences. Reducing the number of collisions and coalescences decreases the number of cells generated; however, claiming that a fewer number of cells will produce more precipitation is not prudent at this time (Rosenfeld 2008) considering the precipitation flux per cell results (Fig. 29). If storms were longer in duration and larger in size, then perhaps Fig. 29 should show a statistically significant increase in precipitation flux per cell with increases in AOD. There may be an artificial effect on cell duration due to the limited radar coverage area, which would then have an effect on precipitation flux per day. Longer duration cells may pass out of the coverage area during their lifetime and not be counted; therefore, total precipitation flux for a day would then be less. Perhaps, the potential loss in precipitation flux per day would be offset because an equal number of cells would also be expected to pass into the analysis region. The sensitivity of the radar's range on cell totals and precipitation flux was not tested. Results only partially support claims made by Jiang and Feingold's (2006) modeling study of the effects that aerosols could have on precipitation. Their modeling results showed that increasing the number concentration of accumulation mode aerosols suppresses surface precipitation by decreasing the average cloud droplet size and efficiency of the collision-coalescence process. While results presented in Chapter IV show that precipitation flux per day decreases as AOD increases (Fig. 31), the slope is not statistically significant.

Project leaders within the weather modification community could use AOD as a decision-making tool because of the significant inverse linear relationship found between cells-per-day and AOD. For example, a project leader could predict narrower drop size distributions within clouds because of measurements on a day indicating higher AE (non-

desert dust) and AOD. Then, the potential reduction in the efficiency of the collision-coalescence process in non-precipitating clouds could be augmented utilizing hygroscopic seeding, increasing the likelihood of a larger areal coverage of surface precipitation. Though, at this time, the fact that there is considerable variability (Figs. 29-32) in these preliminary results warrants more research and evaluation. The following future work would be helpful to understand better the relationship between aerosols and simple cell convection:

1) Use the numerous AERONET and Radar sites located in the United States of America to perform more comparisons similar to the ones presented in Chapter IV.

2) Examine the effects that the 240 km separation distance between the Bamako, Mali radar and the IER Cinzana AERONET site had on the results of the research.

3) Separate analysis into days of unorganized and organized convection.

4) Perform co-located AERONET and CCN measurements over many years and all seasons.

5) Measure CCN directly at cloud base with aircraft based instruments and compare to radar derived precipitation totals for that cell.

6) Test for the significance of the apparent relationship between AE and cells per day.

REFERENCES

Adeyewa, Z. D., and E. E. Balogun, 2003: Wavelength dependence of aerosol optical depth and the fit of the Angstrom law. *Theoretical and Applied Climatology, 74*, 105-122.

Adler, R. F., G. J. Huffman, S. Curtis, and E. J. Nelkin, 2000: Tropical rainfall distributions determined using TRMM combined with other satellite and rain gauge information. *Journal of Applied Meteorology, 39*, 2007-2023.

Albrecht, B. A., 1989: Aerosols, cloud microphysics, and fractional ckoudiness. *Science, 245*, 1227-1230.

Andreae, M. O., 2009: Correlation between cloud condensation nuclei concentration and aerosol optical thickness in remote and polluted regions. *Atmospheric Chemistry and Physics, 9*, 543-556.

ASCE, 2004: *Standard practice for the design and operation of precipitation enhancement projects.* Reston: American Society of Civil Engineers.

Ba, M. B., R. Frouin, and S. E. Nicholson, 1995: Satellite-derived interannual variability of West African rainfall 1983-1988. *Journal of Applied Meteorology, 34*, 411-431.

Bender, R., S. Lange, 2000: Adjusting for multiple testing - when and how?. *Journal of Clinical Epidemiology, 54*, 343-349.

Bland, J. M., D. G. Altman, 1995: Multiple significance tests: the Bonferroni method. *BMJ, 310,* 170.

Bryan, G., 2008: Fortran subroutine to calculate CAPE Version 1.02. UCAR. [Available online at http://www.mmm.ucar.edu/people/bryan/Code/getcape.F.]

Butt, T., B. McCarl, J. Angerer, P. Dyke, and J. Stuth, 2005: The economic and food security implications of climate change in mali. *Climate Change, 68* (3), 355-378.

COMET, cited 2011: Precipitation Estimates, Part 1: Measurement. UCAR. [Available online at http://www.meted.ucar.edu/hydro/precip_est/part1_measurement/print.htm.]

Cotton, W. R., 2007: Basic cloud seeding concepts. *Southwest Hydrology, 6* (2), 16-17.

Delene, D. J., and T. Deshler, 2001: Vertical profiles of cloud condensation nuclei above Wyoming. *Journal of Geophysical Research - Atmospheres, 106,* 12579-12588.

Dennis, A. S., 1980: *Weather Modification by Cloud Seeding* (Vol. 24). New York: Academic Press.

Dixon, M., and G. Wiener, 1993: TITAN: thunderstorm identification, tracking, analysis, and nowcasting-a radar-based methodology. *Journal of Atmospheric and Oceanic Techonology, 10* (6), 785-797.

_____, 2010: TITAN - Thunderstorm identification tracking analysis and nowcasting Version 5. UCAR. [Available online at http://www.ral.ucar.edu/projects/titan/download/perform_download.php.]

Eck, T. F., B. N. Holben, J. S. Reid, O. Dubovik, A. Smirnov, N. T. O'Neill, et al., 1999: Wavelength dependence of the optical depth of biomass burning, urban, and desert dust aerosols. *Journal of Geophysical Research, 104* (D24), 31,333-31,349.

GSFC, cited 2012: AERONET's Version 2.0 quality assurance criteria. [Available online at http://aeronet.gsfc.nasa.gov/new_web/PDF/AERONETcriteria_final1.pdf.]

Holben, B. N., D. Tanre, A. Smirnov, T. F. Eck, I. Slutsker, N. Abuhassan, et al., 2001: An emerging ground-based aerosol climatology: aerosol optical depth from AERONET. *Journal Of Geophysical Research, 106* (D11), 12.067-12.097.

_____, 2012: AERONET Data Download Tool, Version 2 Direct Sun Algorithm [Available online at http://aeronet.gsfc.nasa.gov/cgi-bin/webtool_opera_v2_new.]

Jiang, H., and G. Feingold, 2006: Effect of aerosol on warm convective clouds: aerosol-cloud-surface flux feedbacks in a new coupled large eddy model. *Journal of Geophysical Research, 111*.

Jefferson, A., 2010: Empirical estimates of CCN from aerosol optical properties at four remote sites, Atmos. Chem. Phys., 10, 6855-6861.

Kucera, P. A., D. Delene, M. B. Chapman, S. Hermann, and R. Bruintjes, 2008: *Feasbility study for the augmentation of rain in Mali.* Boulder: National Center for Atomspheric Research.

Le Barbe, L., L. Thierry, and D. Tapsoba, 2002: Rainfall variability in West Africa during the years 1950-1990. *Journal of Climate, 15*, 187-202.

Lesins, G., and U. Lohmann, 2003: GCM aerosol radiative effects using geographically varying aerosol sizes deduced from AERONET measurements. *Journal of the Atmospheric Sciences, 60*, 2747-2763.

Levin, Z., and W. R. Cotton, 2009: *Aerosol pollution impact on precipitation: a scientific review.* Heidelberg and Karlsruhe, Germany: Springer.

Mather, G. K., 1991: Coalescence enhancement in large multicell storms caused by the emissions from a Kraft paper mill. *Journal of Applied Meteorology, 30*, 1134-1146.

Nicholson, S. E., B. Some, and B. Kone, 2000: An analysis of recent rainfall conditions in West Africa, including the rainy seasons of the 1997 E1 Nino and the 1998 La Nina years. *Journal of Climate, 13* (14), 2628-2640.

_____, 2001: Climate and environmental change in Africa during the last two centuries. *Climate Research, 14*, 123-144.

_____, and J. P. Grist, 2003: On the seasonal evolution of atmospheric circulation over West Africa and Equatorial Africa. *Journal of Climate, 16*, 1013-1030.

_____, 2005: On the question of "recovery" of the rains in the West African Sahel. Journal of Arid Environments. *Journal of Arid Environments, 63*, 615-641.

_____, 2009: A revised picture of the structure of the "monsoon" and land ITCZ over West Africa. *Climate Dynamics, 32* (7), 1155-1171.

Nowofor, O. K., 2010: Rising dust aerosol pollution at Ilorin in the sub-sahel inferred from 10-year AERONET data: possible links to persisting drought conditions. *Research Journal of Environmental and Earth Sciences, 2* (4), 216-225.

O'Neill, N. T., T. F. Eck, B. N. Holben, A. Smirnov, and O. Dubovik, 2001: Bimodal size distribution influences on the variation of Angstrom derivatives in spectral and optical depth space. *Journal of Geophysical Research, 106* (D9), 9787-9806.

Pinker, R. T., G. Idemudia, and T. O. Aro, 1994: Characteristic aerosol optical depths during the Harmattan season in sub-Saharan Africa. *Geophysical Research Letters, 21* (8), 685-688.

Pruppacher, H. R., and J. D. Klett, 1997: *Microphysics of clouds and precipitation* (2nd ed.). Kluwer.

Rogers, R. R., and M. K. Yau, 1989: *Short Course in Cloud Physics* (3rd Edition ed.). Oxford and New York: Pergamon Press.

Rosenfeld, D., U. Lohmann, G. B. Raga, C. D. O'Dowd, M. Kulmala, S. Fuzzi, et al., 2008: Flood or drought: how do aerosols affect precipitation? *Science, 321*, 1309-1313.

Sauvageot, H., and J. P. Lacaux, 1995: The shape of averaged drop size distributions. *Journal of the Atmospheric Sciences, 52*, 1070-1083.

Silverman, B. A., 2003: A critical assesment of hygroscopic seeding of convective clouds for rainfall enhancement. *Bulletin of the American Meteorological Society, 84*, 1219-1230.

Sultan, B., and S. Janicot, 2000: Abrupt shift of the ITCZ over West Africa and intra-seasonal variability. *Geophysical Research Letters, 27*, 3353-3356.

_____, and S. Janicot, 2003: West African monsoon dynamics. Part II: The "pre-onset" and the "onset" of the summer monsoon. *Journal of Climate, 16*, 3407-3427.

Toledano, C., M. Wiegner, M. Garhammer, M. Seefeldner, J. Gasteiger, D. Muller, et al., 2009: Spectral aerosol optical depth characterization of desert dust during SAMUM 2006. *Tellus, 61B*, 216-228.

Twomey, S., 1974: Polution and the planetary albedo. *Atmospheric Envrionment, 8*, 1251-1256.

Weisman, M. L., and J. B. Klemp, 1982 The dependence of numerically simulated convective storms on vertical wind shear and bouyancy. *Monthly Weather Review, 110*, 504-520.

Zhang, C., P. Woodworth, and G. J. Gu, 2006: The seasonal cycle in the lower troposphere over West Africa from sounding observations. *Quarterly Journal of the Royal Meteorological Society, 132*, 2561-2584.